Evaluation of the Performance of a Short-Span T-Beam Bridge

Final Report
September 2021

BRIDGE ENGINEERING CENTER



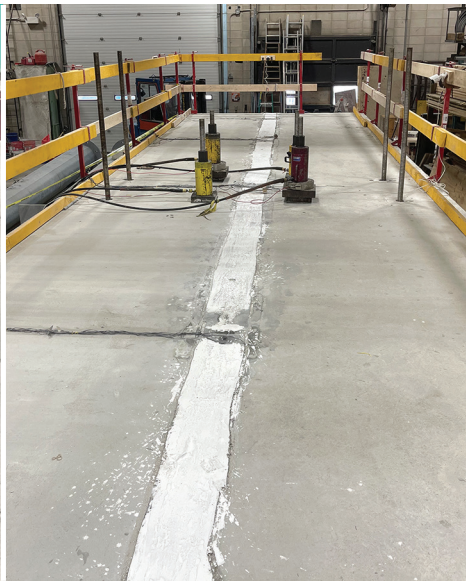

IOWA STATE UNIVERSITY
Institute for Transportation

Sponsored by
Iowa Highway Research Board
(IHRB Project TR-705)
Iowa Department of Transportation
(InTrans Project 16-572)

About the Bridge Engineering Center

The mission of the Bridge Engineering Center (BEC) is to conduct research on bridge technologies to help bridge designers/owners design, build, and maintain long-lasting bridges.

About the Institute for Transportation

The mission of the Institute for Transportation (InTrans) at Iowa State University is to save lives and improve economic vitality through discovery, research innovation, outreach, and the implementation of bold ideas.

Iowa State University Nondiscrimination Statement

Iowa State University does not discriminate on the basis of race, color, age, ethnicity, religion, national origin, pregnancy, sexual orientation, gender identity, genetic information, sex, marital status, disability, or status as a US veteran. Inquiries regarding nondiscrimination policies may be directed to the Office of Equal Opportunity, 3410 Beardshear Hall, 515 Morrill Road, Ames, Iowa 50011, telephone: 515-294-7612, hotline: 515-294-1222, email: eooffice@iastate.edu.

Disclaimer Notice

The contents of this report reflect the views of the authors, who are responsible for the facts and the accuracy of the information presented herein. The opinions, findings and conclusions expressed in this publication are those of the authors and not necessarily those of the sponsors.

The sponsors assume no liability for the contents or use of the information contained in this document. This report does not constitute a standard, specification, or regulation.

The sponsors do not endorse products or manufacturers. Trademarks or manufacturers' names appear in this report only because they are considered essential to the objective of the document.

Iowa DOT Statements

Federal and state laws prohibit employment and/or public accommodation discrimination on the basis of age, color, creed, disability, gender identity, national origin, pregnancy, race, religion, sex, sexual orientation or veteran's status. If you believe you have been discriminated against, please contact the Iowa Civil Rights Commission at 800-457-4416 or Iowa Department of Transportation's affirmative action officer. If you need accommodations because of a disability to access the Iowa Department of Transportation's services, contact the agency's affirmative action officer at 800-262-0003.

The preparation of this report was financed in part through funds provided by the Iowa Department of Transportation through its "Second Revised Agreement for the Management of Research Conducted by Iowa State University for the Iowa Department of Transportation" and its amendments.

The opinions, findings, and conclusions expressed in this publication are those of the authors and not necessarily those of the Iowa Department of Transportation.

Technical Report Documentation Page

1. Report No. IHRB Project TR-705	**2. Government Accession No.**	**3. Recipient's Catalog No.**
4. Title and Subtitle Evaluation of the Performance of a Short-Span T-Beam Bridge		**5. Report Date** September 2021 6. Performing Organization Code
7. Author(s) Behrouz Shafei (orcid.org/0000-0001-5677-6324) and Rizwan Karim (orcid.org/0000-0003-4130-568X)		**8. Performing Organization Report No.** InTrans Project 16-572
9. Performing Organization Name and Address Bridge Engineering Center Iowa State University 2711 South Loop Drive, Suite 4700 Ames, IA 50010-8664		**10. Work Unit No. (TRAIS)** **11. Contract or Grant No.**
12. Sponsoring Organization Name and Address Iowa Highway Research Board Iowa Department of Transportation 800 Lincoln Way Ames, IA 50010		**13. Type of Report and Period Covered** Final Report **14. Sponsoring Agency Code** IHRB Project TR-705

15. Supplementary Notes

Visit https://bec.iastate.edu for color pdfs of this and other research reports.

16. Abstract

The secondary road system in Iowa is vitally important to the movement of goods and people throughout the state. In some cases, secondary roads serve as feeders to the primary road system and then on to the National Highway System. In other cases, the secondary road system serves as a critical link for farmers as they move their crops. With approximately 20,000 bridges on the secondary system, county engineers are faced with the ever more difficult task of maintaining and replacing those bridges.

In an effort aimed toward identifying alternative bridge systems, especially for bridges with shorter span lengths, this research project focused on a new bridge girder/deck section that consists of a single T-shape. The individual T-shape sections are connected together using a cast-in place ultra-high performance concrete (UHPC) longitudinal joint. Additionally, the proposed section uses commercially available, corrosion-resistant, reinforcing steel, which has tensile strengths in the order of 130 ksi.

Through a set of laboratory experiments, the behavior of the individual T-beams and a joint setup made with two T-beams was systematically tested in this project under service limit loads for flexure and shear stress. The experimental test results were then utilized to validate finite element (FE) models created using the Abaqus software package. The FE models were employed to investigate the behavior of the joint under various loading scenarios.

The results from the experiments and FE simulations showed that the proposed joint detailing and bridge system performed well under service limit loads for both flexure and shear. With the combination of strength and durability advantages introduced, the outcome of this research project is expected to help county engineers consider the new bridge system developed as a promising alternative for short-span bridges.

17. Key Words bridge girder/deck section—corrosion-resistant rebar—experimental tests—finite element modeling—high-strength rebar—longitudinal joints—T-beams—ultra-high performance concrete		**18. Distribution Statement** No restrictions.	
19. Security Classification (of this report) Unclassified.	**20. Security Classification (of this page)** Unclassified.	**21. No. of Pages** 59	**22. Price** NA

Form DOT F 1700.7 (8-72) **Reproduction of completed page authorized**

EVALUATION OF THE PERFORMANCE OF A SHORT-SPAN T-BEAM BRIDGE

Final Report
September 2021

Principal Investigator
Behrouz Shafei, Associate Professor
Bridge Engineering Center, Iowa State University

Co-Principal Investigator
Brent Phares, Research Structural Engineer
Bridge Engineering Center, Iowa State University

Research Assistant
Rizwan Karim

Authors
Behrouz Shafei and Rizwan Karim

Sponsored by
Iowa Highway Research Board and
Iowa Department of Transportation
(IHRB Project TR-705)

Preparation of this report was financed in part
through funds provided by the Iowa Department of Transportation
through its Research Management Agreement with the
Institute for Transportation
(InTrans Project 16-572)

A report from
Bridge Engineering Center
Iowa State University
2711 South Loop Drive, Suite 4700
Ames, IA 50010-8664
Phone: 515-294-8103 / Fax: 515-294-0467
https://bec.iastate.edu

TABLE OF CONTENTS

LIST OF FIGURES

ACKNOWLEDGMENTS

The authors would like to thank the Iowa Highway Research Board (IHRB) and Iowa Department of Transportation (DOT) for sponsoring this research project.

The reinforcing steel bar used for the laboratory investigations were received from MMFX Technologies Corporation. This support is gratefully acknowledged.

The authors would also like to thank the staff of the Structural Engineering Research Laboratory at Iowa State University for their support in performing the experimental work.

EXECUTIVE SUMMARY

The secondary road system in Iowa is vitally important to the movement of goods and people throughout the state. In some cases, secondary roads serve as feeders to the primary road system and then on to the National Highway System. In other cases, the secondary road system serves as a critical link for farmers as they move their crops. With approximately 20,000 bridges on the secondary system, county engineers are faced with the ever more difficult task of maintaining and replacing those bridges.

In an effort aimed toward identifying alternative bridge systems, especially for bridges with shorter span lengths, this research project focused on a new bridge girder/deck section that consists of a single T-shape. The individual T-shape sections are connected together using a cast-in place ultra-high performance concrete (UHPC) longitudinal joint. Additionally, the proposed section uses corrosion-resistant, high-strength reinforcing steel.

Through a set of laboratory experiments, the behavior of the individual T-beams and a joint setup made with two T-beams was systematically tested in this project under service limit loads for flexure and shear stress. The experimental test results were then utilized to validate finite element (FE) models created using the Abaqus software package.

The FE models were employed to investigate the behavior of the joint under various loading scenarios. The results from the experiments and FE simulations showed that the proposed joint detailing and bridge system performed well under service limit loads for both flexure and shear stress.

With the combination of strength and durability advantages introduced, the outcome of this research project is expected to help county engineers consider the new bridge system developed as a promising alternative for short-span bridges.

1. INTRODUCTION

1.1 Background

Precast bridge elements can result in better quality production, faster construction, and possibly reduction in overall cost. Among the examples of precast beam elements are box beam girders, deck bulb T-beams, and T-beams. These beams are connected together at their flanges by a longitudinal joint.

Longitudinal joints are often required in wide bridges, although state recommendations vary about the width of the individual bridge decks (Phares et al. 2015). These longitudinal joints are considered a vulnerable region, which can result in structural deterioration and reduction in the service life of bridges. The common problems associated with these longitudinal joints are cracking within filler materials, reflective cracking, and leakage in the joint (Jones et al. 2015). The leakage in the joint allows for chloride-contaminated water to seep through to the reinforcing steel bars and the underlying structure, leading to corrosion.

The current literature available on the choice of material and the detailing of longitudinal joints for T-beams is limited. Meanwhile, the development of new construction materials is inspiring engineers and researchers to develop construction-friendly, durable, and smaller-sized bridge girder/deck sections.

1.2. Literature Review

Longitudinal joints have been a subject of interest for many state departments of transportation (DOTs). The Nebraska DOT (NDOT) had a welded connection with two 4 in. steel plates anchored in the concrete deck. The two plates were welded to a steel bar in the joint (Figure 1(a)).

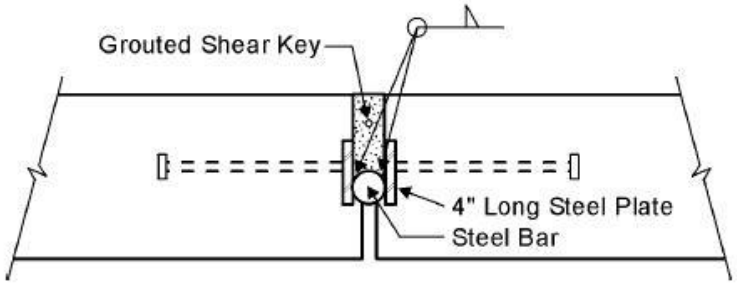

Martin and Osborn 1983, FHWA

(a)

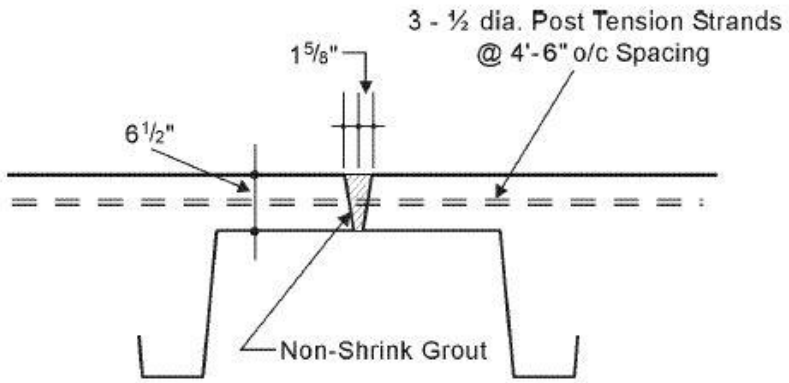

El Shahawy 1990, *PCI Journal*

(b)

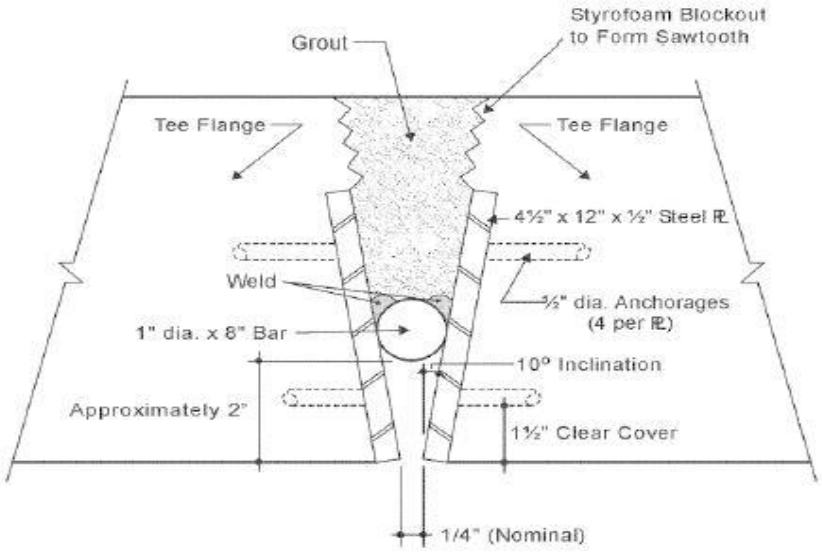

Jones 2001, Texas Transportation Institute

(c)

Figure 1. Simple longitudinal joint details from (a) Nebraska DOT, (b) Florida DOT, and (c) Texas DOT

The connection was then filled with grout. These types of transverse connections were placed every 4–6 ft, center to center (Martin and Osborn 1983).

The Florida DOT (FDOT) had a continuous longitudinal grouted V-joint for bridges with heavy traffic (Figure 1(b)). The joint was post-tensioned by utilizing the reinforcing steel bar extending across the joint in the transverse direction (El Shahaway 1990).

Other types of connection details include welded plates joints, which are similar to the details from NDOT, except that the steel plates are welded to another plate instead of a steel bar. The Texas DOT (TxDOT) built on the previous work of the design from NDOT and developed a simple connection detail (Jones 2001). The connection has inclined steel plates anchored in the

concrete deck, which are then welded to a 1 in. rod in the joint (Figure 1(c)). Unlike the NDOT detail, which has a smooth surface along the depth of the joint, the TxDOT connection has a saw-tooth finish that allows for a better connection between the joint material and the deck concrete. The connections were required every 5 ft, center to center.

Ultra-High Performance Concrete as the Joint Material

With the advancements in joint filler and reinforcing steel bar materials, attempts have been made to make the joint details simpler, more durable, and more construction-friendly. The joint filler materials need to have high strength, adequate bonds with existing or new concrete decks, and good durability properties.

Latex-modified concrete (LMC) has been utilized as a filler material in the past (Wenzlick 2006, Baer 2013). Latex is a portland cement additive that helps in reducing the water required, thus improving workability. Latex in concrete helps in reducing the number of voids and microcracks by forming an elastic membrane within the concrete matrix.

Magnesium ammonium phosphate (MAP) grout is another type of material used as a joint filler (Gulyas et al. 1995). MAP grout is used because of properties such as less permeability, ability to cure internally, and excellent freeze-thaw resistance.

Wehbe et al. (2016) found non-shrink grout effective for longitudinal joints. Shrinkage-compensating cement concrete, which helps in the reduction of cracking at early stages of hydration, has also been found to be effective for application in longitudinal joints (Shi et al. 2019 and 2020a–c, Liu et al. 2020). Fiber-reinforced concrete (FRC) and ultra-high performance concrete (UHPC) are other two types of cementitious composites that can offer great durability and post-cracking performance. Various efforts have been made in the development and application of FRC for bridge structures (e.g., Dopko et al. 2018 and 2020, Shafei et al. 2021, Karim and Shafei 2021a). Similarly, efforts have gained momentum in the development and application of UHPC in bridge structures (e.g., Karim et al. 2019, Karim and Shafei 2021 b, Oppong et al. 2021, DeJong et al. 2021).

UHPC is gaining more and more attention as a joint filler material. UHPC offers superior strength, durability, and crack resistance capabilities (Graybeal 2010, 2014). Graybeal, (2010) evaluated six different specimens with UHPC connections. Four of those specimens represented connections between precast deck panels and two represented connections between deck bulb T-girders. The connection between the two deck bulb T-girders had two different types of reinforcing steel bar: headed mild steel and straight mild steel (Figure 2).

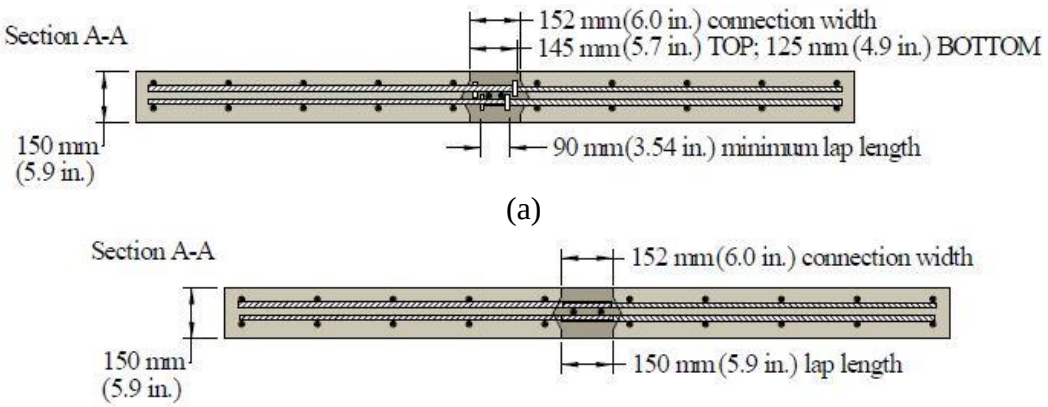

Graybeal 2014, FHWA

Figure 2. Longitudinal UHPC connection details: (a) with headed reinforcing steel bars and (b) with straight mild reinforcing steel bars

The thickness of the head on the headed reinforcing steel bar was 12.7 mm (0.5 in.) and had a diameter of 50.47 mm (1.988 in.). The headed reinforcing steel bars had a minimum overlap length of 88.9 mm (3.5 in.), and the straight reinforcing steel bars had a minimum overlap of 149.9 mm (5.9 in.). The adjacent non-contact spliced reinforcing steel bars were spaced at 88.9 mm (3.5 in.) apart. Two additional #5 reinforcing steel bars went along the joint longitudinally between the heads of the reinforcing steel bars in both details. The joint was a diamond shaped female-female shear key with a width of 152.4 mm (6 in.) at the top and bottom.

The specimens were tested with point loading at the midspan right at the connection between the deck and the joint. The study concluded that the connection between the UHPC joint and high-performance concrete (HPC) panels did not show any debonding; similarly, no debonding of the lapped reinforcing steel bars was observed.

Bohn (2017) tested two joints rehabilitated with large-scale beams to evaluate LMC and UHPC for joint details in double T-beams. The beams tested were 12.19 m (40 ft) long and 1.17 m (3.83 ft) wide. The study investigated two types of longitudinal joint concepts: pocket and continuous. The pockets were rehabilitated with UHPC and the continuous joint was rehabilitated with LMC. The study found that the bridge joint did not experience any cracking beyond initial shrinkage cracking and recommended using UHPC as a potential filler material. The study concluded that rehabilitation of double T-beams utilizing pockets could save up to 70% of the cost of bridge replacement.

Peruchini et al. (2017) studied UHPC as the longitudinal joint material for deck bulb T-beams. The beams were connected flange to flange using a UHPC joint. The transverse reinforcing steel bars from the deck were extended into the joint (Figure 3).

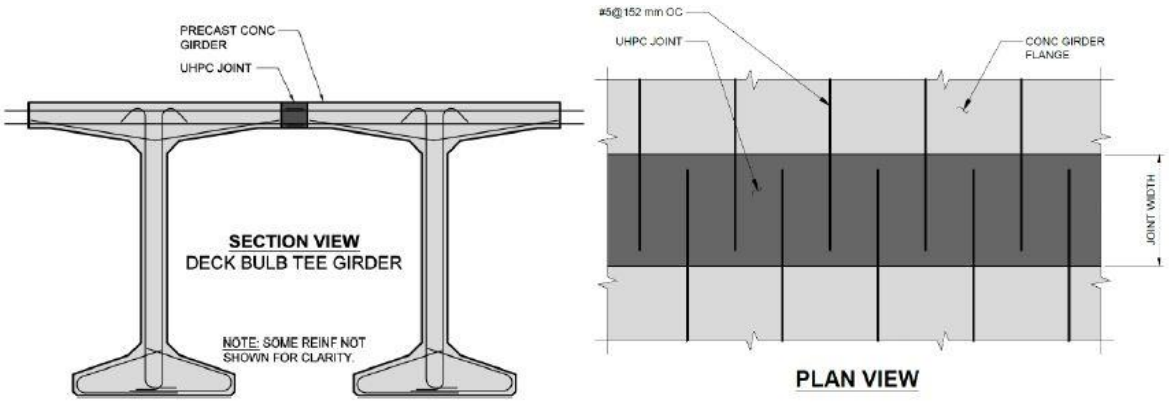

Peruchini et al. 2017, Washington State Transportation Center

Figure 3. UHPC longitudinal joint details in deck bulb T-beam

The UHPC utilized was a non-proprietary UHPC mixture developed at the University of Washington. The study explored different geometries of the joint utilizing finite element (FE) models. After preliminary analysis, a set of deck panels joined by UHPC joints was tested. The panels were 0.60 m (2 ft) wide and 2.44 m (8 ft) long. The deck panels were made of concrete and represented the flange of a bulb T-beam.

The joint was tested with static loading at the midpoint. The variables in the test included the width of the joint, the type of splicing for the reinforcing steel bars in the joint, and the bar offset.

The results from the study showed that the strength of the joint increased in wider joints and smaller offsets. The study also found that the no-contact splicing performed better than contact splicing of the reinforcing steel bars in the joint. A joint width of 22.86 cm (9 in.) would provide sufficient strength for the developed non-proprietary UHPC mixture.

The current availability of information on UHPC as a longitudinal joint material is scarce. The few studies available also differ in the detailing of joints and the methods of testing. The lack of full-scale test specimens is another factor, because the material and structural behavior of UHPC longitudinal joints in T-beams is not completely understood.

Corrosion-Resistant Reinforcing Steel Bars

Corrosion of reinforcing steel bars is a major problem in transportation infrastructures exposed to aggressive environmental stressors (Khatami and Shafei 2021, Khatami et al. 2021). The corrosion of reinforcing steel bar results in the need for regular maintenance and loss of capacity over time. Corrosion becomes increasingly important with bridge structures, given they are exposed to extreme weather year-round, and a small crack can give way to deicing chemicals, which results in rapid corrosion of steel reinforcement.

Among corrosion-resistant reinforcing steel bars, ChromX is produced using a controlled-rolling production procedure. These bars are made from a chromium alloy with low carbon content. The

unique production process and chemical composition result in a corrosion-resistant microstructure. The corrosion in conventional steel starts because of carbides and ferrites, which form a microgalvanic cell in the presence of moisture. In ChromX reinforcing steel bars, the formation of this microgalvanic cell is minimized by a microstructure that resembles the formation of layers of plywood (Gong et al. 2002).

ChromX reinforcing steel bars are a product of martensitic microcomposite formable steel (MMFX) technology. The steel bars come in the ChromX 9000, 4000, and 2000 series. They vary slightly in strength and chromium content. Past studies conducted on ChromX reinforcing steel bars have largely focused on their resistance against corrosion and the effect of temperature on the behavior of these bars (Gong et al. 2002, Dougherty et al. 2009, Farid et al. 2020).

A detailed study by Frosch et al. (2014) compared 10 types of corrosion-resistant reinforcing steel bars with a carbon black reinforcing steel bar. These reinforcing steel bars included MMFX reinforcing steel bars as well. The MMFX reinforcing steel bars showed comparable bond strengths to the carbon black reinforcing steel bars, while epoxy-coated reinforcing steel bars showed reduced bond strength.

The study also found that concrete samples made with MMFX reinforcing steel bars resulted in similar crack widths as those made with the carbon black reinforcing steel bars. At stresses greater than 80 ksi, the crack widths increased nonlinearly for both stainless steel and MMFX reinforcing steel bars.

The study also reported that the deck specimens with top reinforcing steel bars made of corrosion-resistant material and with bottom reinforcing steel bars made of carbon black resulted in the formation of galvanic cells within the deck and, thus, the bottom reinforcing steel bars corroded faster. The study recommended that decks should be made with high-strength, corrosion-resistant materials.

Sharp et al. (2011) summarized the acceptance criteria and quality assurance in the use of high-strength, corrosion-resistant reinforcing steel bars for structural application purposes. Sharp and Moruza (2009) compared the installation and placement cost of MMFX and epoxy-coated reinforcing steel bars. The study reported the construction of two similar bridge decks for the Virginia DOT (VDOT). One deck was made with epoxy-coated reinforcing steel bars while the other deck was reinforced with MMFX reinforcing steel bars. The study concluded that, although the epoxy-coated bars are less costly per unit, the additional cost of handling, transportation, and maintenance results in an increased final cost than that for MMFX reinforcing steel bars. Thus, the study recommended corrosion-resistant reinforcing steel bars over epoxy-coated reinforcing steel bars.

1.3. Research Overview

This study evaluated MMFX reinforcing steel bars for full scale T-beam bridges with a UHPC joint. The T-beam’s flanges form the deck, and the UHPC longitudinal joint joins these T-beams

at their flanges to make a full-sized bridge. This unique setup provides new information on designing T-beams, especially for short-span bridges.

This report presents the results from a full-scale test of two concrete T-beams joined by a UHPC longitudinal joint. The T-beams utilized high-strength, corrosion-resistant steel bars for reinforcement. These reinforcing steel bars had tensile strength greater than 910.1 MPa (132 ksi). The reinforcing steel bars were extended from the deck into the UHPC joint. The longitudinal joint and the bridge system were tested under flexure and shear stress. The T-beams were then individually tested by cutting through the joint and separating the beams. A set of FE models were created from the laboratory-tested bridge elements to further evaluate the use of the proposed bridge girder/deck section in bridge setups under the maximum moment created by an HL-93 truck.

1.4 Research Study Benefits

The results of this research deliver original information about the performance of T-beams reinforced with high-strength, corrosion-resistant reinforcing steel bars. In addition, new insight is provided regarding the stress distribution within the longitudinal joint under flexure and shear loading. This will aid in the design of UHPC longitudinal joints, especially for short-span T-beam bridges.

2. EXPERIMENTAL SETUP AND TESTING PLAN

The goal of the experimental investigation was to evaluate a full system made of T-beams and a uniquely designed longitudinal joint. The full-scale experimental specimen consisted of two T-beams joined through a longitudinal UHPC joint. The entire test setup was 14.0 m (46 ft) long and 3.7 m (12 ft) wide (Figure 4).

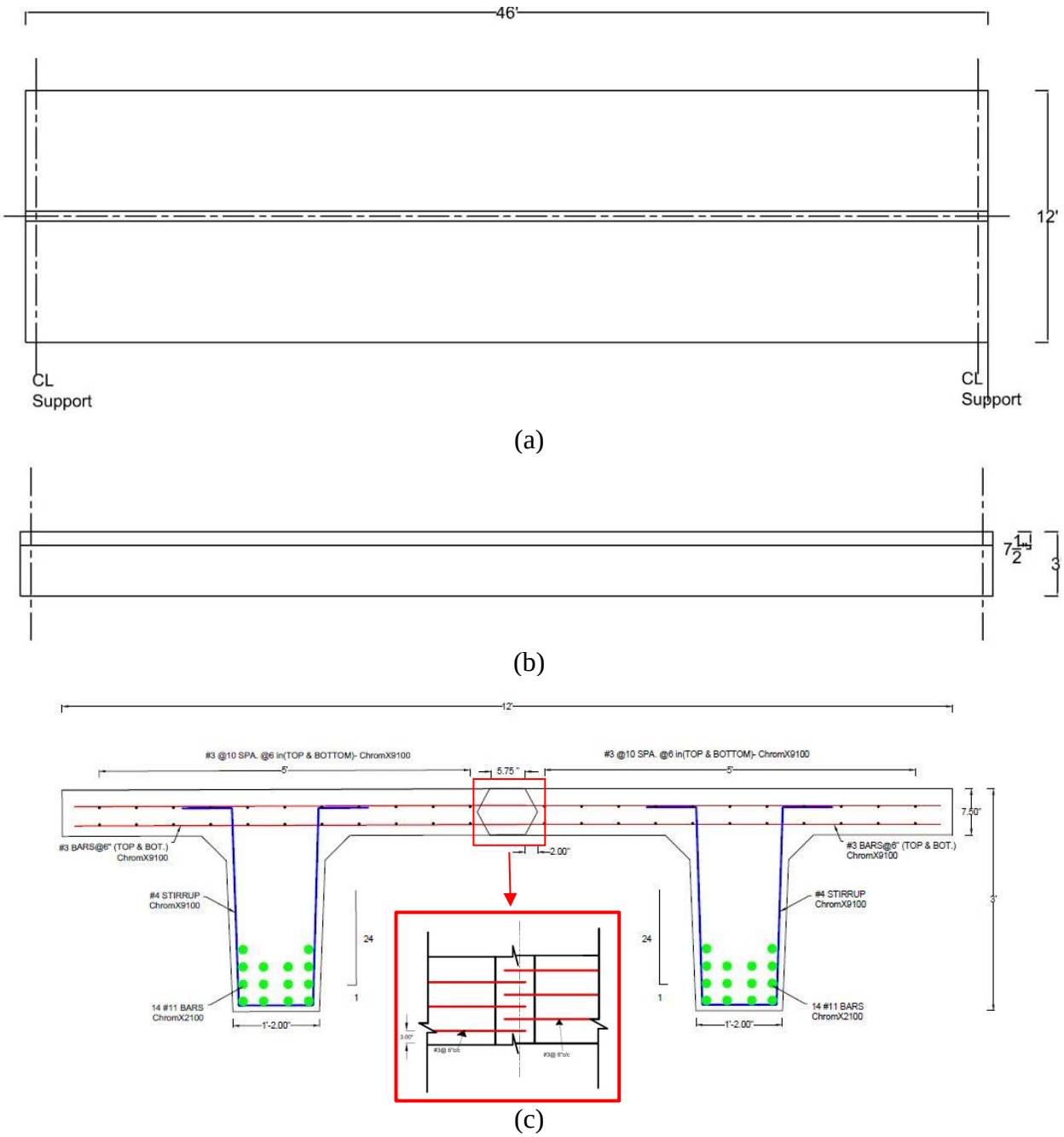

Figure 4. (a) Plan, (b) elevation, and (c) section view of the specimen

The individual beams were 14.0 m (46 ft) long with a clear span of 13.7 m (45 ft). The beam flanges were 1.76 m (5.76 ft) wide and 19.05 cm (7.5 in.) deep. The total depth of each beam was 91.44 cm (36 in.), with 19.05 cm (7.5 in.) of flange and 72.39 cm (28.5 in.) of web. The thickness of the web varied with 35.56 cm (14 in.) at the bottom and 40.64 cm (16 in.) at the height of 60.96 cm (24 in.). The slope of the sides was 24:1. The remaining 10.16 cm (4 in.) of the web was tapered out at a slope of 1:1 before becoming part of the flange.

Each beam had 14 #11 ChromX 2100 reinforcing steel bars at the bottom. These reinforcing steel bars were corrosion resistant. The reinforcing steel bars had a yield strength of 913.5 MPa (132.5 ksi) and ultimate strength of 1,200.3 MPa (174.1 ksi) with an elongation capacity of 9% according to the datasheet provided by the manufacturer. The high strength allows for construction of T-beams without the need for prestressing.

The stirrups were made of #4 reinforcing steel bars with ChromX 9100. These reinforcing steel bars had a yield strength of 885 MPa (128.2 ksi) and ultimate tensile strength of 1127 MPa (163.3 ksi). The stirrups were spaced at 15.24 cm (6 in.) for the first 1.83 m (6 ft) from the supports, 20.32 cm (8 in.) for the next 2.44 m (8 ft), 30.48 cm (12 in.) for the next 1.83 m (6 ft) and 45.72 cm (18 in.) for the remaining distance (3 ft) to midspan. The spacing of the stirrups was symmetric about the midspan.

The deck reinforcing steel bars were all #3 ChromX 9100. The reinforcing steel bars were spaced at 6 in. in both the longitudinal and transverse directions. The reinforcing steel bars had a yield strength of 933 MPa (135.2 ksi) and ultimate strength of 1,145 MPa (165.9 ksi). The top and bottom transverse reinforcing steel bars coming from the deck extended into the joint to 6.35 cm (2.5 in.) past the centerline of the joint. The reinforcing steel bars coming from both sides resulted in a staggered configuration with 7.62 cm (3 in.) spacing between them and provided a no-contact splice of 12.7 cm (5 in.).

The concrete in the T-beam was a C4 chip mix with a smaller aggregate size (maximum of 19.05 mm [3/4 in.]) to allow for it to flow smoothly between the congested spaces between the bottom reinforcing steel bars. The mix resulted in 6.7 ksi 28-day compressive strength. The individual beams required 13 yd^3 of concrete to pour. The construction images of the first beam are shown in Figure 5.

(a)

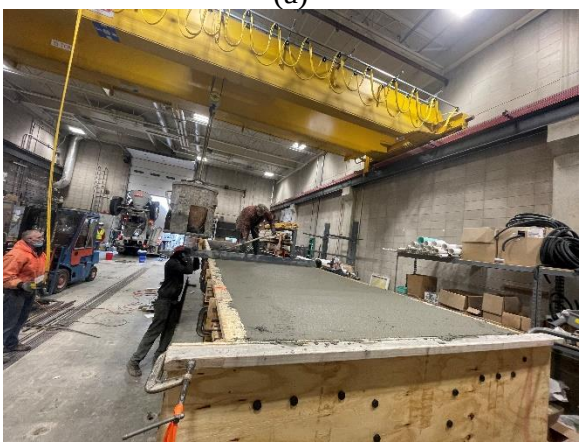

(b)

(c)

Figure 5. (a) Rebar mat, (b) pouring of concrete, and (c) poured beam specimen

The images show the rebar mat, the pouring process, and first beam after pouring the concrete.

The joint between the two beams was filled with UHPC mixed in the laboratory. A total of 20 ft^3 of UHPC mix was required for the joint. The required UHPC was mixed in five batches of 4 ft^3. The UHPC mix resulted in a 28-day strength of 18 ksi for the samples that were kept in the laboratory to simulate the condition of the joint without any curing. The samples kept in the

curing room resulted in 22 ksi compressive strength at 28 days. The joint was also divided into five sections to pour each batch separately, as shown in Figure 6.

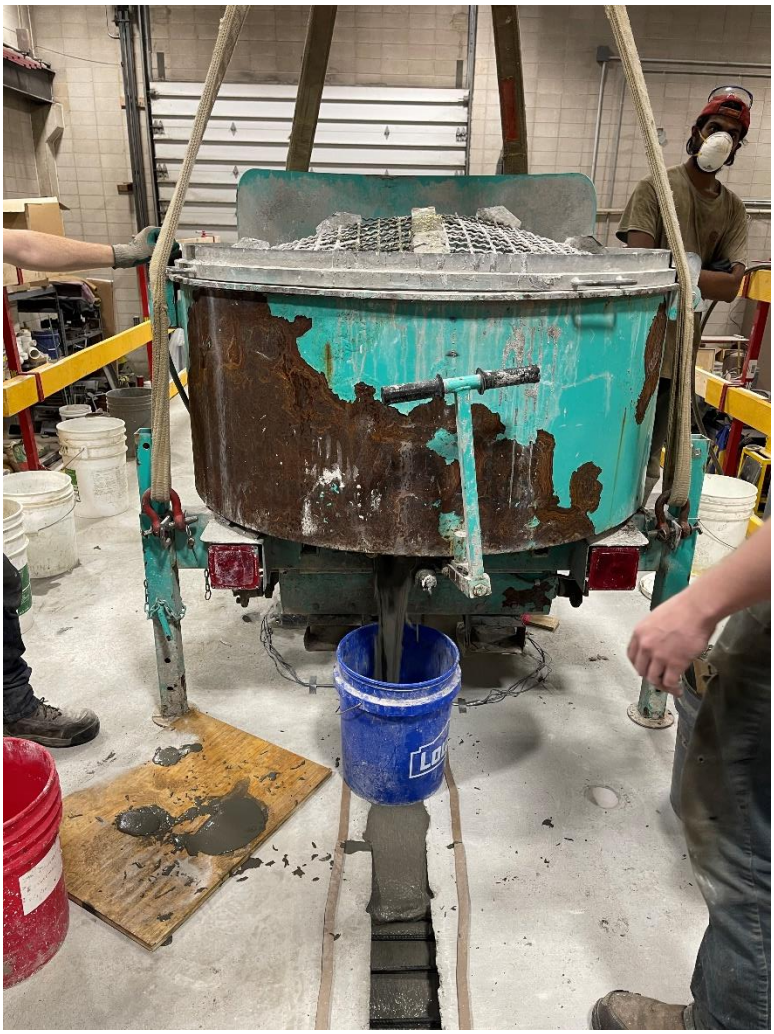

Figure 6. Pouring of UHPC joint section

2.1. Instrumentation

The specimen was instrumented with a dense network of gauges: BDI strain transducers, direct current displacement transducers (DCDTs), and linear variable differential transformers (LVDTs). Based on the identified locations of interest, the three types of strain gauges were reinforcing steel bar strain gauges, embedded concrete strain gauges, and surface strain gauges.

The three critical sections that were identified for instrumentation were the midspan of the bridge and the quarter span on each side of midspan, as detailed in Figure 7.

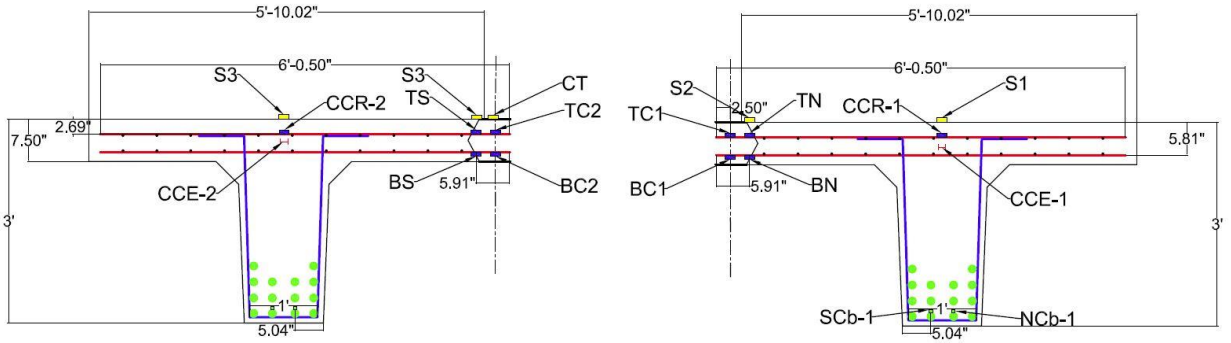

Section View at Midspan For Beam-2

Section View at Midspan For Beam-1

(a)

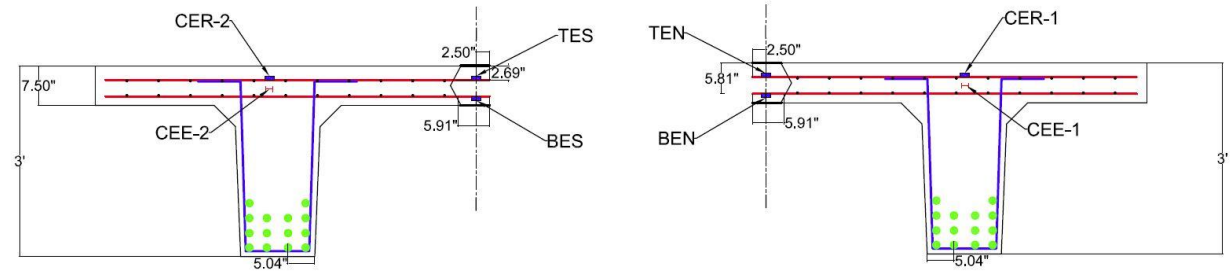

Section View at Quarter Span Beam 2-East End

Section View at Quarter Span Beam 1-East End

(b)

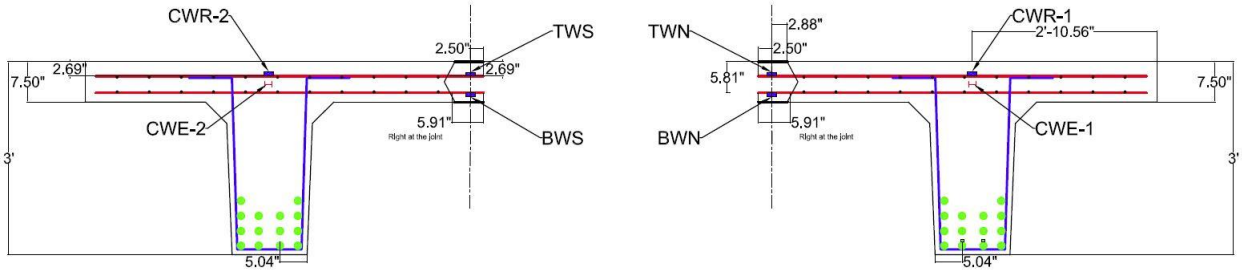

Section View at Quarter Span beam 2-West End

Section View at Quarter Span Beam 1-West End

(c)

Solid blue rectangles = strain gauges on the rebar, red horizontal I shapes = embedded strain gauges, and solid yellow rectangles = surface strain gauges

Gauges in the beams with same name but ending in 1 are on beam 1 (south beam) and ending in 2 are on beam 2 (north beam).

Middle letter E = east quarter span and W = west quarter span.

First letter N or S = north or south, respectively.

First letter T or B = top or bottom for joint strain gauges and second letter C, N, or S = center of joint, north of joint, or south of joint, respectively.

Figure 7. Instrumentation plan for the tests

The midspan had strain gauges at the bottom longitudinal reinforcing steel bar of the beam at midspan, strain gauges on the top transverse reinforcing steel bar of the deck, and embedded strain gauges in the transverse direction in the deck.

Surface strain gauges were placed on top of the beam on the deck and at the same locations in both the transverse and longitudinal directions. Two additional surface strain gauges were placed just next to the joint on the top surface of the deck.

DCDTs were extended across the top of the joint to record any crack width formation. The joint had surface strain gauges on the top and BDI strain gauges on the bottom reinforcing steel bars—at center and at the interface of the joint and the concrete.

Strain gauges were placed at quarter span at the top transverse reinforcing steel bar of the deck and embedded in the transverse direction. Surface strain gauges were placed on the deck at quarter span on each side right next to the joint. The joint had reinforcing steel bar strain gauges on both the top and bottom reinforcing steel bars. The top surface had strain gauges in both the transverse and longitudinal directions.

Reinforcing steel bar strain gauges were mounted on the stirrups close to supports to capture the performance of the stirrups, since the shear strain would be maximum at this location. Surface strain gauges were also instrumented on top of the joint in the transverse direction. LVDTs were installed at the bottom of the beam at midspan and quarter span to record the deflection of the beam.

2.2. Test Plan

The entire structure was tested utilizing eight loading points, with four loading points on each beam. Only four points were loaded at a time using four 978.6 kN (220 kip) capacity actuators, with the tests systematically carried out to explore four unique load cases as follows.

In case 1, the outer two loading points on each beam were loaded within service limit loads. The anticipated loading in the joint was tensile stresses on the top and compressive stresses on the bottom of the joint (see Figure 8).


Data Acquisition Center
Actuators

(a)

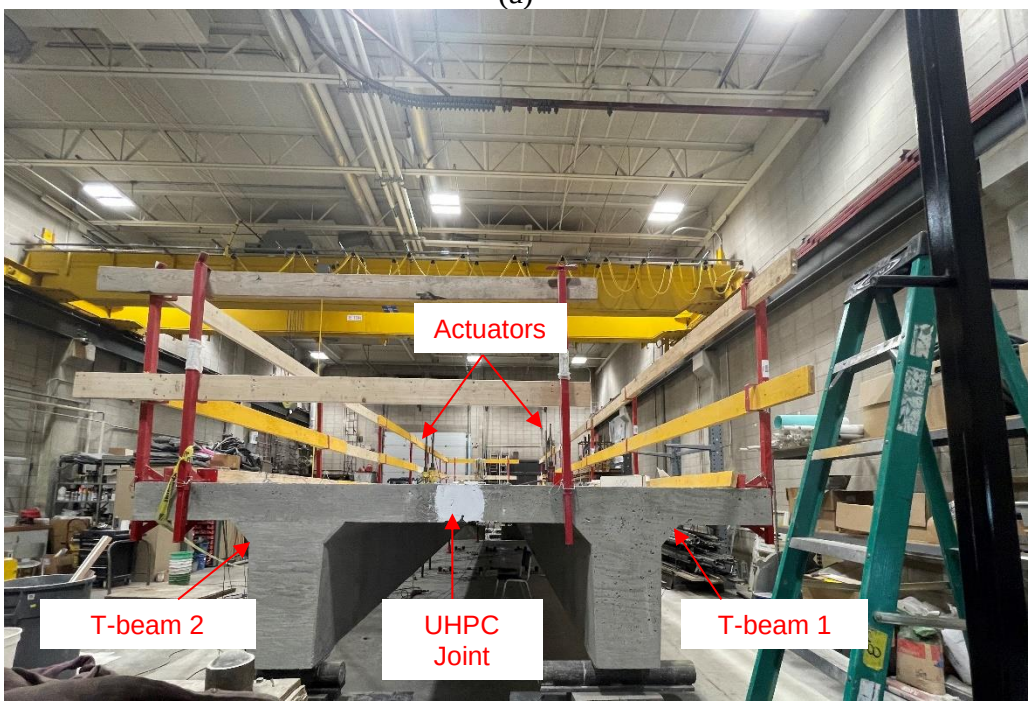
Actuators
T-beam 2
UHPC Joint
T-beam 1

(b)

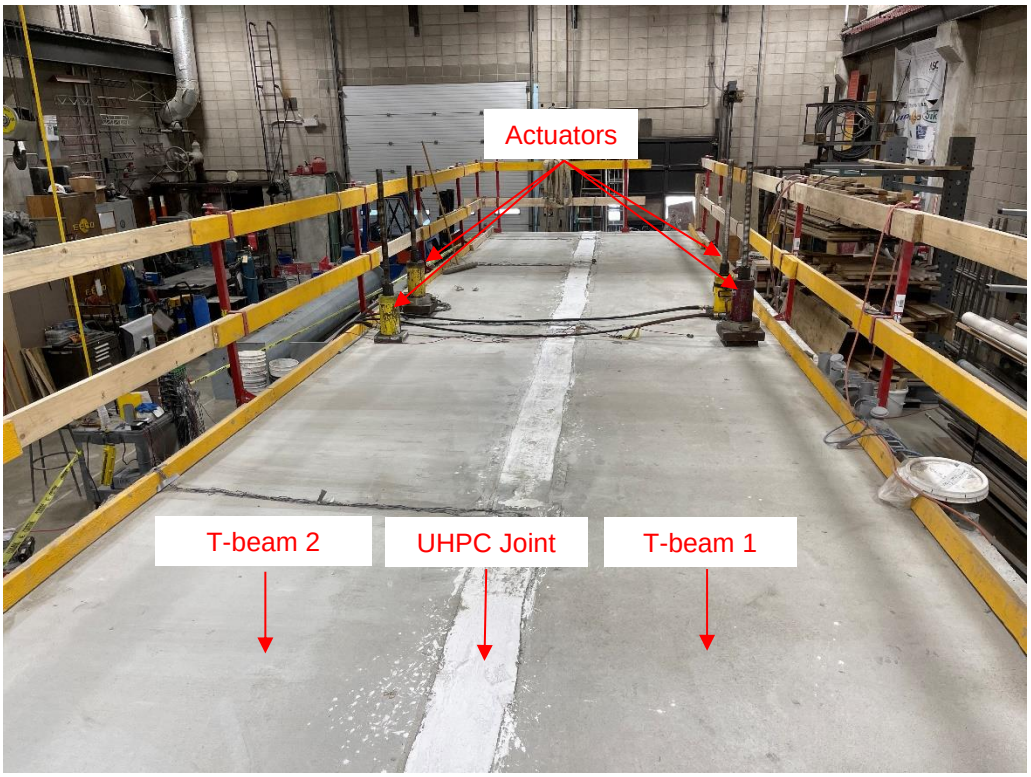

(c)

Figure 8. (a) Longitudinal, (b) cross sectional, and (c) top view for case 1

In case 2, the inner two loading points on each beam were loaded within service limit. The anticipated loading in the joint was compression on top of the joint and tension in the bottom surface of the joint. In these first two cases, the loading on the joint was flexure (see Figure 9(a)).

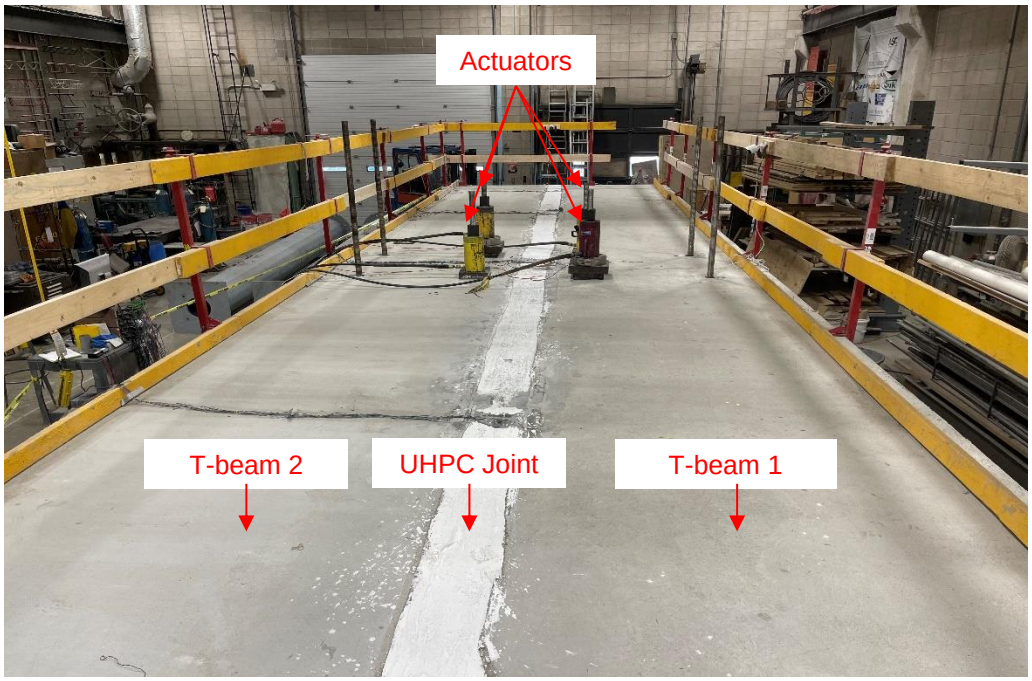

(a)

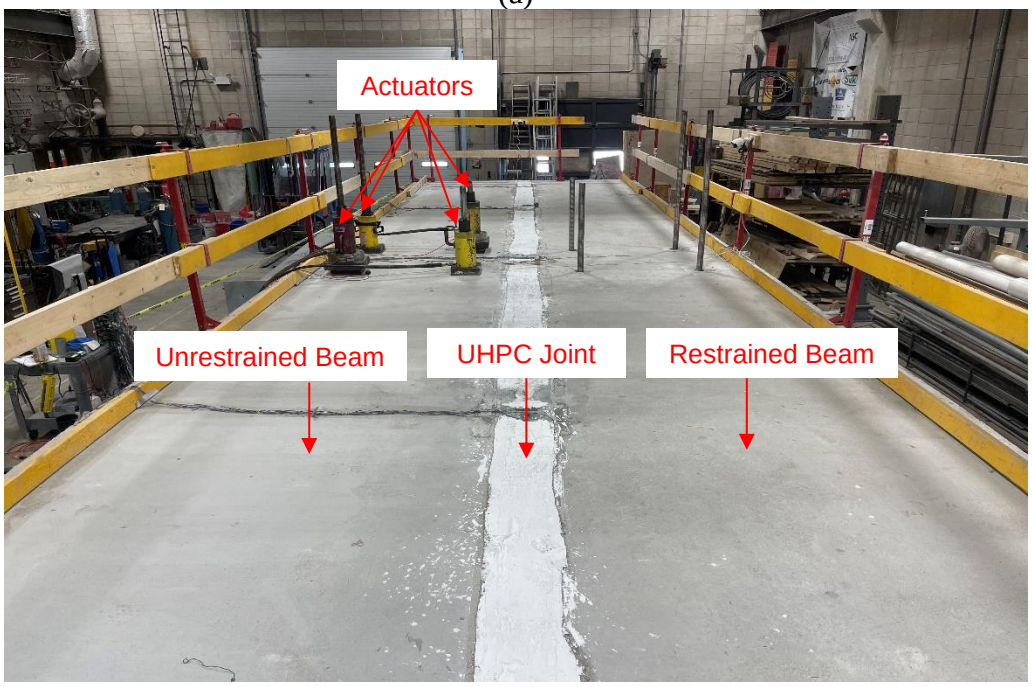

(b)

Figure 9. (a) Loading scenario in case 2 (b) loading scenario in case 3

In case 3, the loading was applied to introduce maximum shear stresses in the joint. To achieve this goal, the deflection of one of the beams was restrained by placing additional support under the beam along the length of the beam (see Figure 9(b)).

These restraints were provided by placing steel I-beams under the loading points and then additional supports in the form of jacks at quarter span. These supports only restrained the movement of the beam in the vertical direction. The second beam was loaded at all four points to exert the highest shear force in the joint.

The first three cases were only for service limit loads. The service limit load for a two-span, 46 ft long bridge was determined to be 41.2 kips across each loading line (20.6 kips on each loading point) for the current loading arrangement. All three cases were tested for 21 kips loading on each loading point.

After the case 3 test, the two beams were separated by cutting through the center of the UHPC joint using a saw for case 4. The two beams were separated, and the restraints under the first beam were removed. The two beams were separately tested to investigate the behavior of T-beams under flexure. The test results help understand the behavior of the individual T-beams under flexural loading.

3. RESULTS AND DISCUSSION FOR EXPERIMENTAL TESTING

The results obtained from the four test cases described in the previous chapter are presented in this chapter. The force, deflection, strain, and crack width results were monitored utilizing the dense distribution of gauges. The DCDTs did not record any data because there were no cracks for service limit loadings in the joint or on the deck.

3.1. Case 1: Outer Two Points Loaded

For case 1, the outer two loading points on each beam were loaded up to the service limit of 21 kips (a total of 42 kips). The load deflection data were monitored for these loadings (Figure 10(a)).

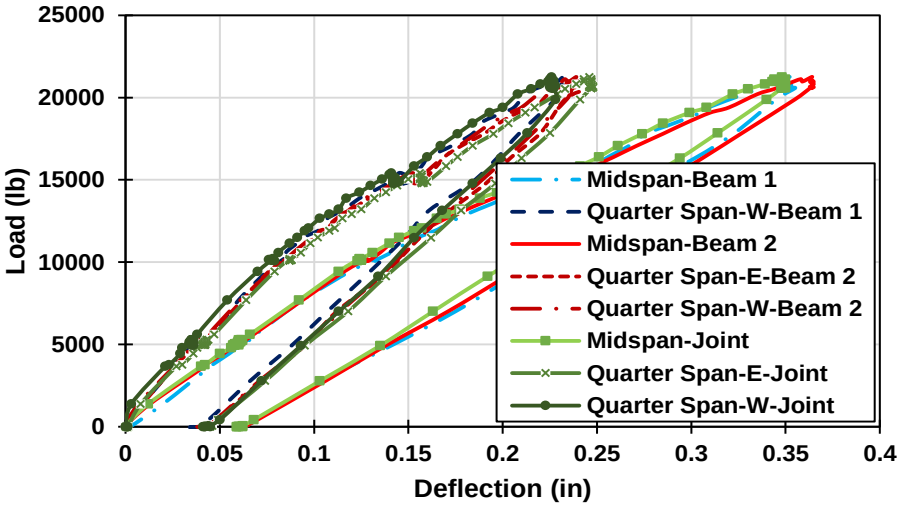

(a)

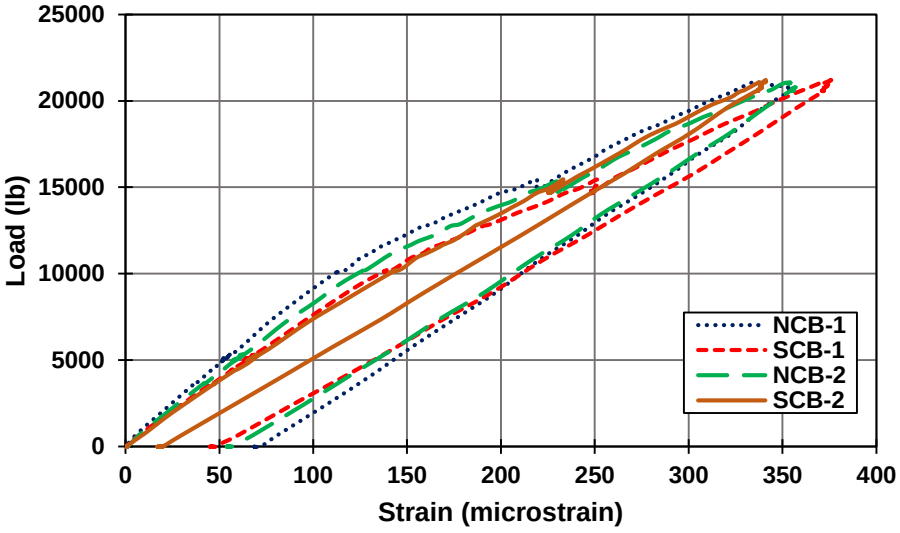

Figure 10. (a) Load deflections and (b) load strains for case 1

The load deflection data show that the beam behavior was linear elastic up to a 10 kips load, when a change of slope was observed. The load deflection behavior that stayed linear until 21 kips loading became a slope lower than the initial slope after that. The midspan and quarter span load deflection curves for each beam followed an almost similar path, highlighting the fact that the loading was symmetric and that both beams behaved in similar ways. The unloading curves also followed a similar smooth unloading curve. The observations from load deflection curves were complemented by the load strain curves for strains recorded at the bottom reinforcing steel bars of both beams at midspan (Figure 10(b)). Similar to the load deflection curves, the load strain curves also changed slope around 10 kips loading and stayed linear until the 21 kips loading, but with reduced slope.

The strains were recorded on the surface of the joint, in the joint reinforcing steel bar, and on the concrete deck adjacent to the joint. These values were recorded at midspan and quarter spans. Midspan had the largest number of strain gauges to measure all strains across the section of the bridge to measure transverse strains (Figure 11).

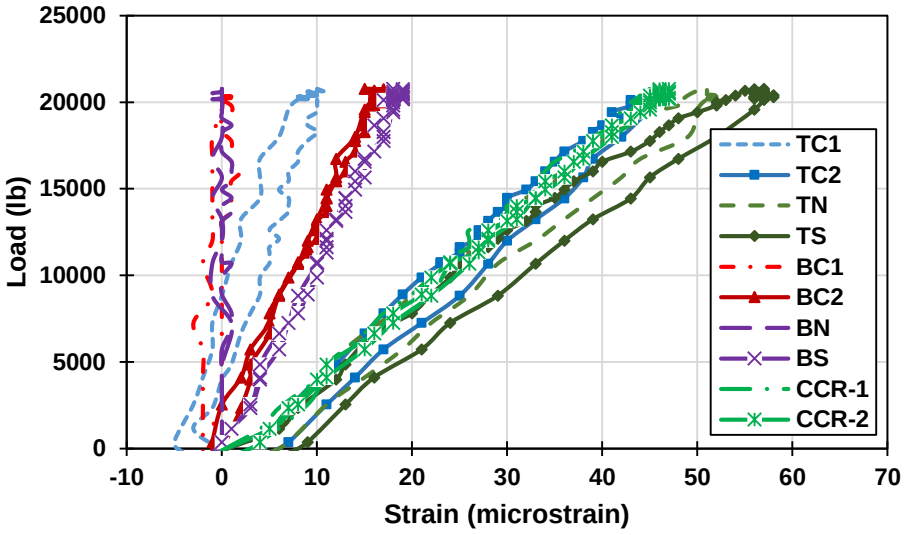

(a)

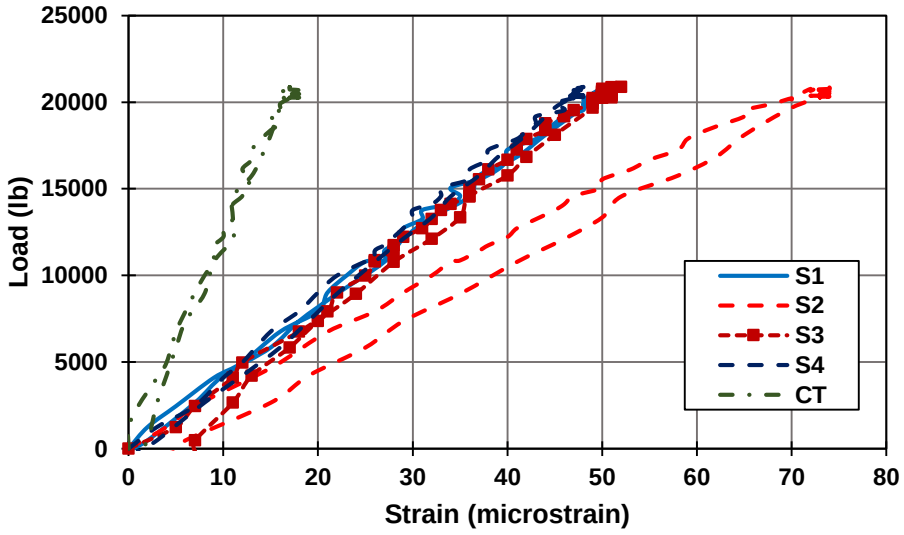

(b)

Figure 11. Load strains for (a) transverse strain in top and bottom rebars and (b) surface strains at midspan for case 1

The strains recorded on the reinforcing steel bar in the deck show that all strains remained at very low values, i.e., less than 50 microstrain. The strain in the top reinforcing steel bars in the joint (i.e., TC1 and TC2) and deck (i.e., CCR-1 and CCR-2) was tensile while the strain in the bottom reinforcing steel bars was compressive for initial loading of 5 kips and then started to become tensile, as well; this indicates a more complex distribution of loading rather than a simple tensile load on top and compression at the bottom loading anticipated in the initial phase of loading. The tensile strain in both the bottom (i.e., BC1 and BC2) and top (i.e., TC1 and TC2) reinforcing steel bars indicated that the joint was under a combined action of flexural and axial loading. The joint was in pure flexure at lower values of loading (for loading below 5 kips) but at higher values of loading as the stress in the reinforcing steel bars in the joint became purely axial. The strain gauges located at the interface of the UHPC joint and the concrete beams, i.e.,

TN, TS, BN, and BS, also resulted in tensile strains. This indicated that the entire joint was under tensile forces. The two T-beams started to behave as a pivot for the loading points, and the joint was under purely axial stress in the transverse direction.

The integrity of the UHPC joint and the connection between joint UHPC and concrete beams were also closely monitored by installing DCDTs across the joint on the top and bottom of the joint. The DCDTs did not record any data, indicating no cracking in the joint and no separation of the connection between the UHPC joint and the concrete beams. Detailed visual inspection was carried out during and after loading to check for any cracking in the joint or on the deck, and no cracks were observed.

The strains in the reinforcing steel bars were complemented with strain recorded on the surface of the joint and on the deck at midspan. The strain-load presented in Figure 11(b) shows the surface strains recorded. S1 and S4 were located at the middle of the cross section of beam 1 and 2, respectively. S2 and S3 were located 2 in. from the joint on the top surface of the deck, and gauge CT was the transverse direction strain gauge on top of the UHPC joint. The strains recorded on the joint were much lower than the strain recorded on the concrete deck right next to the joint. The strain recorded by the CT gauge was 15 microstrain, while that recorded by the S2 and S3 gauges was 74 and 53 microstrain, respectively. This highlights the ability of the UHPC joint to resist elongation.

The strains were measured at the quarter span as well. The instruments were installed both east and west of center. The strains recorded for the top and bottom reinforcing steel bars followed the same pattern as that recorded for the strain at midspan. The strain recorded in the top reinforcing steel bars recorded at quarter span were about one fifth of that recorded for the strains at midspan (Figure 12).

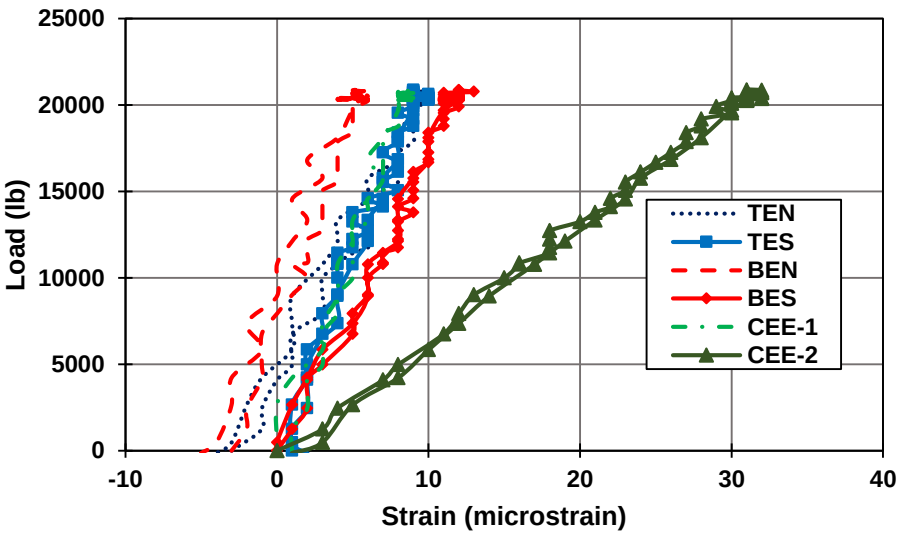

(a)

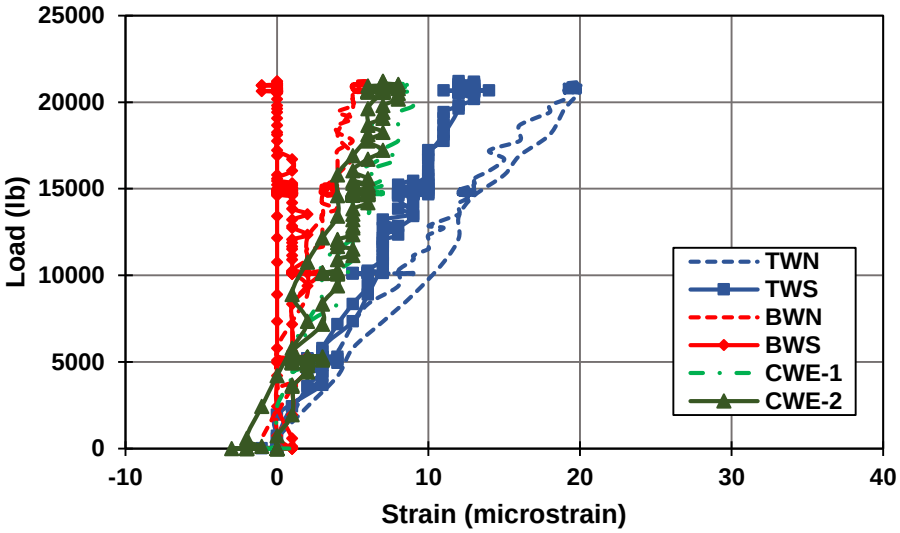

(b)

Figure 12. Transverse rebar strains for (a) east quarter span and (b) west quarter span for case 1

All strains recorded were equal to or less than 10 microstrain, except for CEE-2, which showed exceptionally higher strain values than the other strain gauges. The strain gauge locations of CEE-1 and CEE-2 is the same and should have resulted in similar strain values. The observations from CWE-1 and CWE-2 show that the CEE-2 results were unexpectedly high and may not accurately represent the actual behavior. All strains at the quarter span were around 15 microstrain; whereas, the strains recorded at midspan were as high as 50 microstrain in the joint and 70 microstrain in the deck. This shows that, when moving away from the center of the joint, the strains started to decrease.

3.2. Case 2: Inner Two Points Loaded

In this test setup, the two inner points on each beam were loaded with an anticipation that it would result in tensile stresses at the bottom and compressive stresses at the top of the joint (Figure 8(a) in the previous chapter). The deflection was recorded at the bottom of the beam at midspan and quarter span. The load deflection curve is shown in Figure 13(a).

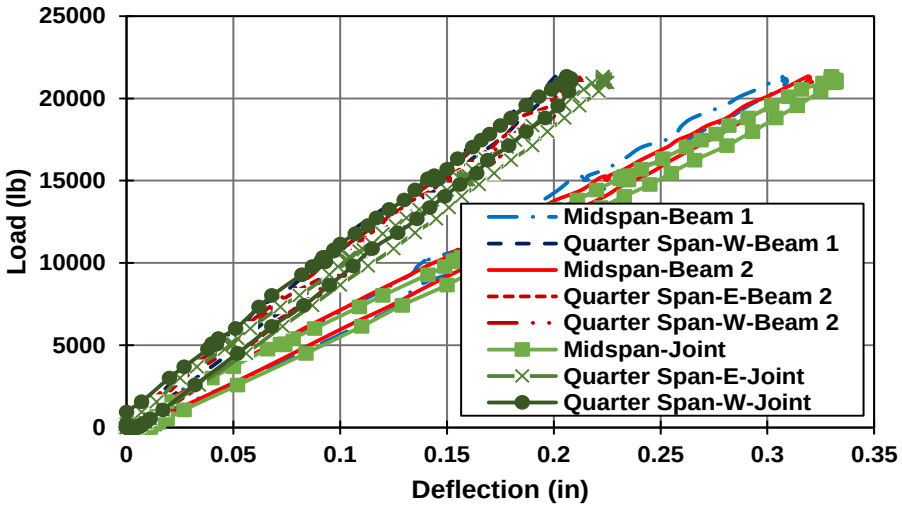

(a)

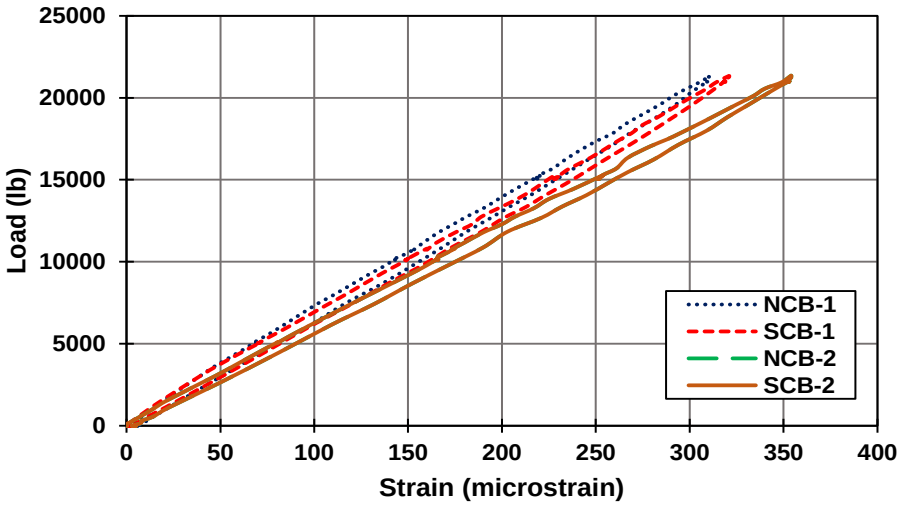

(b)

Figure 13. (a) Load deflections for midspan and quarter span and (b) load strains at the bottom rebars of the beams for case 2

The recorded loads are for the loading at individual points. The load deflection curves show that the behavior stayed linear elastic. The setup came back to almost the same position, and the residual deflection was only 0.02 in. at midspan. No cracks were observed in the beams. The load deflection behavior showed a linear elastic behavior until 21 kips loading at each point and a smooth unloading curve was observed with no negligible residual measured deflection. Midspan and quarter span deflections resulted in the same behavior for both beams. The load strain curves recorded for the strains in the bottom reinforcing steel bars of the beams showed similar behavior as the load deflection curves (Figure 13(b)). SCB-1 and NCB-1 were at midspan at the bottom reinforcing steel bars and SCB-2 and NCB-2 were at the bottom reinforcing steel bars of beam 2 at midspan. The load strain curves were linear elastic during loading and

unloading. The strain resulted in almost the same strain values as those for case 1 (i.e., 350 microstrain).

The strains were also recorded in the transverse direction at the mid-section in the transverse direction. The strains recorded in the top reinforcing steel bars were compressive and the bottom reinforcing steel bars experienced tensile strain (Figure 14).

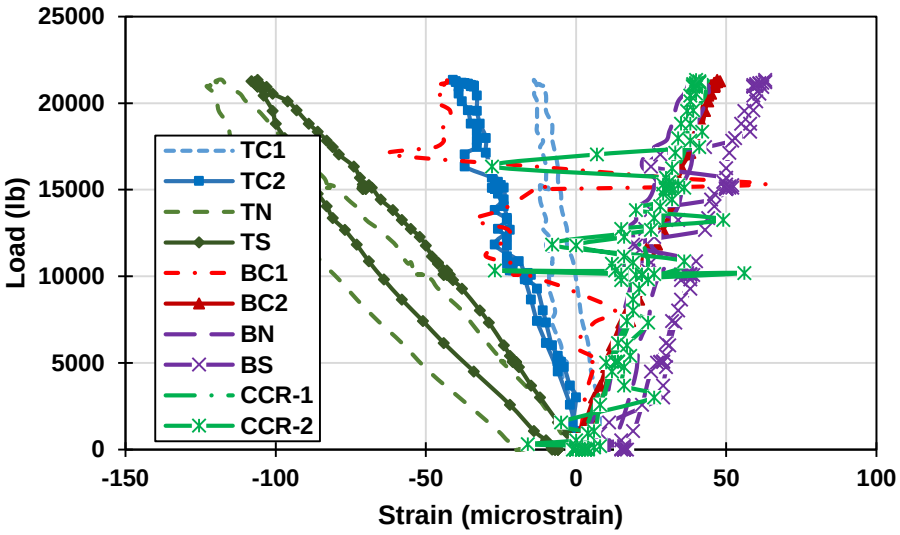

(a)

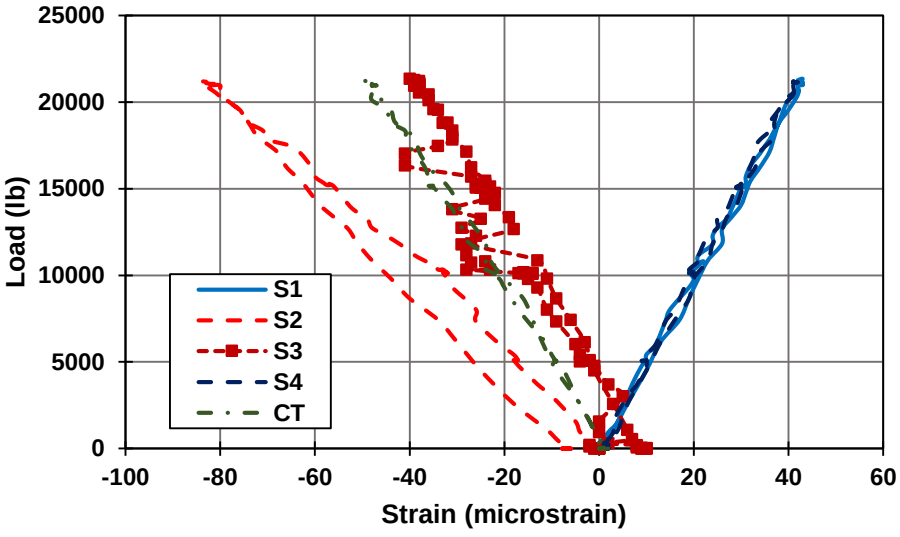

(b)

Figure 14. Load strains for (a) transverse strains in top and bottom rebars and (b) surface strains at midspan for case 2

The top TC1, TC2, TS, and TN reinforcing steel bars experienced compressive strains. The strains recorded at the center of the joint (i.e., TC1 and TC2) were lower than the strain recorded at the interface of the UHPC joint and the concrete beams. The bottom reinforcing steel bars

experienced tensile strains, as anticipated. The tensile strains at the center of the joint (i.e., BC2) were lower than the strains recorded at the interface of the joint and the concrete beam (i.e., BS and BN). The strains in the top reinforcing steel bars in the deck were also compressive and resulted in almost the same strain as the strain at gauge BN. BC1 and CCR-2 recorded strain data may not be accurate as presented in the figure, and an accurate assumption could be made by observing results from BC2 and CCR-1, as they were at the corresponding position in the other beam. The tensile strains in case 2 were slightly lower than those observed for case 1, but the compressive strains were significantly higher than those for case 1.

The strains recorded at the surface of the deck and joint are presented in Figure 14(b). It can be seen that all strain gauges located in between the loading point (i.e., CT on the joint and S2 and S3 on the deck) resulted in compressive strains, while the two strain gauges located on top of the deck, outside the loading points S1 and S4, resulted in tensile strain. Unlike case 1, the strain recorded in the joint was relatively high, i.e., 50 microstrain in case 2 compared to 18 microstrain in case 1. The strain recorded on top of the joint was compressive as opposed to tensile in case 1, as expected.

The transverse strains were also recorded at quarter span for both beams (on both the east and west side of midspan) (Figure 15).

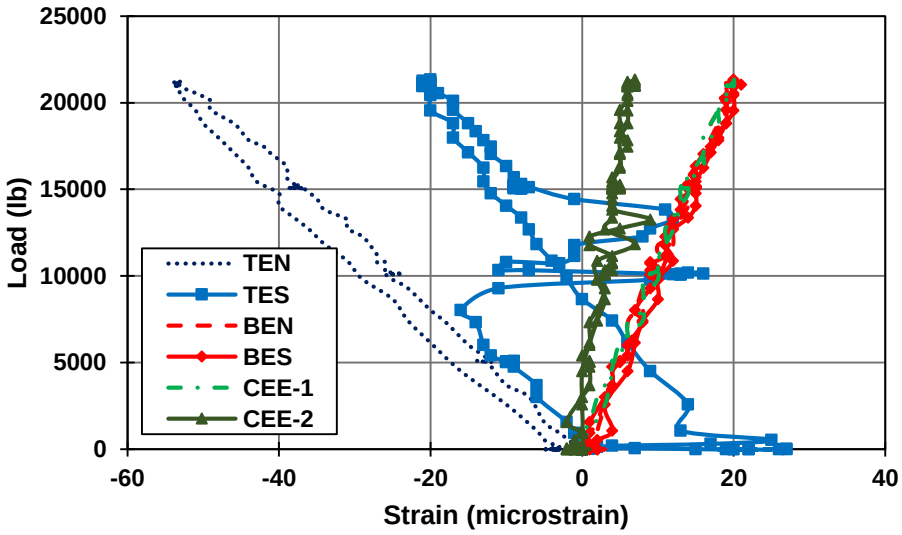

(a)

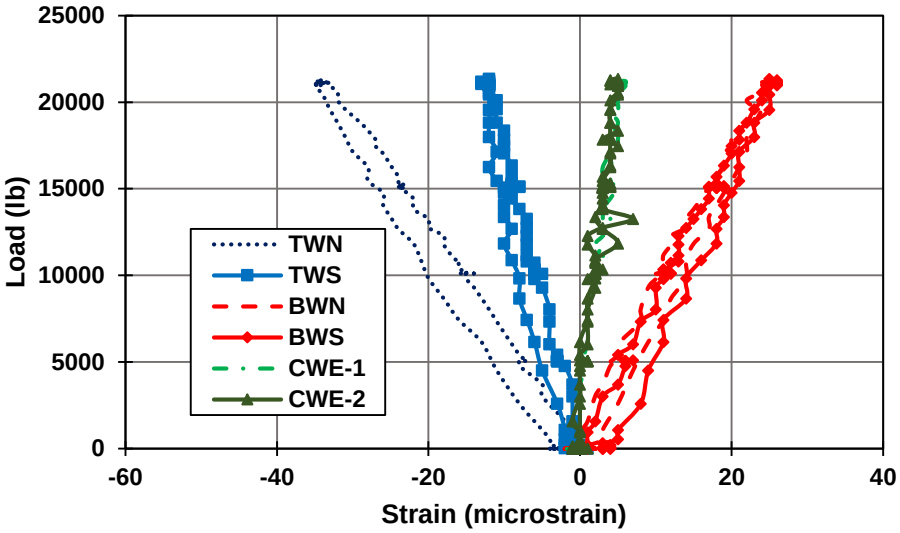

(b)

Figure 15. Transverse rebar strains for (a) east quarter span and (b) west quarter span for case 2

The recorded strain trends were consistent with what was observed for midspan, with top reinforcing steel bars in the joint in compression and bottom reinforcing steel bars in tension. The recorded compressive and tensile strains in the corresponding strain gauges were almost half of what was observed at midspan.

3.3. Case 3: One Beam Restrained and All Points on Other Beam Loaded

The motivation for exploring case 3 was to investigate the joint's behavior under maximum shear force, as the joint acted as a shear key in addition to transferring moments. To maximize shear stress, the vertical movement of one beam was restrained. The unrestrained beam was loaded at all four points. The deflections at midspan and quarter span and the strains in the joint and on the deck were recorded. The load deflections are presented in Figure 16(a).

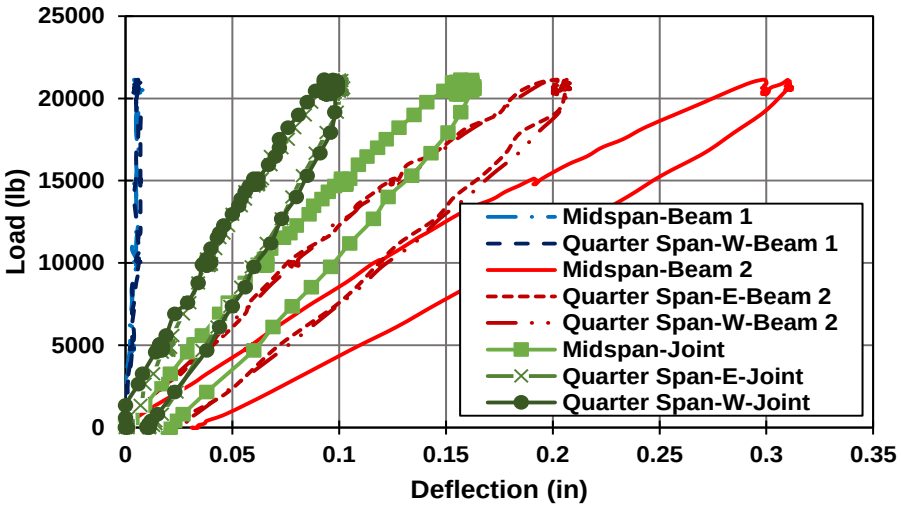

(a)

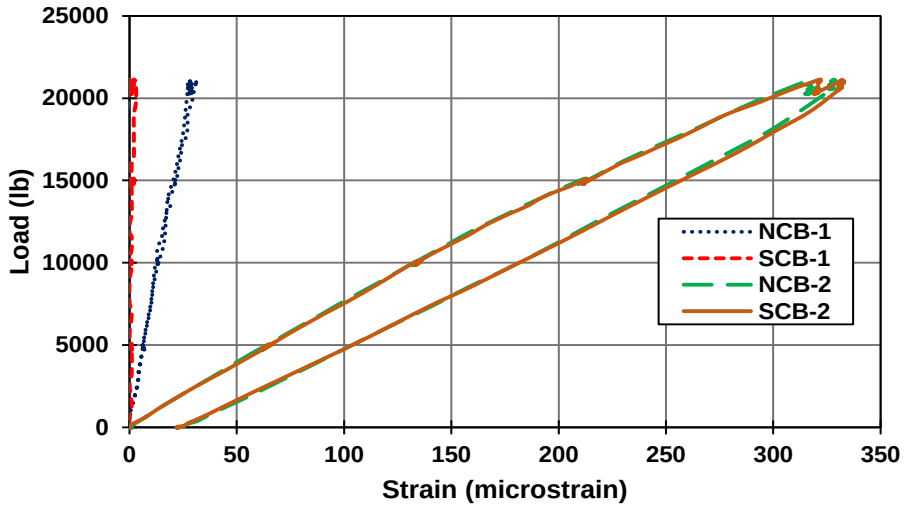

(b)

Figure 16. (a) Load deflections for midspan and quarter span and (b) load strains for bottom rebars of the beams for case 3

The loads presented were at the individual loading points, and the deflections presented were at the bottom of the beams at midspan and at the east quarter span. The east quarter span LVDT in beam 1 did not record data during the testing, and that is why only the west quarter span deflections are presented in the figure. The load deflection curve showed a linear relation until 12 kips; after that, the slope reduced but stayed linear and constant until 21 kips loading. The unloading deflection curve showed a smooth linear relationship with a residual deflection of 0.032 and 0.022 in., respectively. The deflection data were recorded for the restrained beam, as well, and those data showed negligible deflection. The deflections at midspan and quarter span for the restrained beam were 0.003 and 0.002 in., respectively, at 21-kip loading. This shows that the restraint supports were effective in keeping the beam restrained.

The deflection data are further complemented by the strains recorded at the bottom reinforcing steel bars located at midspan of both beams (Figure 16(b)). The strain data show that the strains in the restrained beam, i.e., NCB-1 and SCB-1, were well below the strains recorded for the unrestrained beam, i.e., NCB-2 and SCB-2. The strains for NCB-1 and SCB-1 were 28 and 1 microstrain, respectively, at 21 kips loading. The strain gauges in the unrestrained beam recorded 329 microstrain at the same loading value. The load strain curve for the unrestrained beam remained linear. The load strain curve changed slope at 12 kips but had a constant slope after that until 21 kips. The smooth unloaded curve was recorded with strain gauges in the restrained beam showing no residual strains, while the strain gauges in the unrestrained beams recorded 25 microstrain.

The load strain curves for the transverse strain gauges at midspan on the reinforcing steel bars in the joint and on the deck are presented in Figure 17(a).

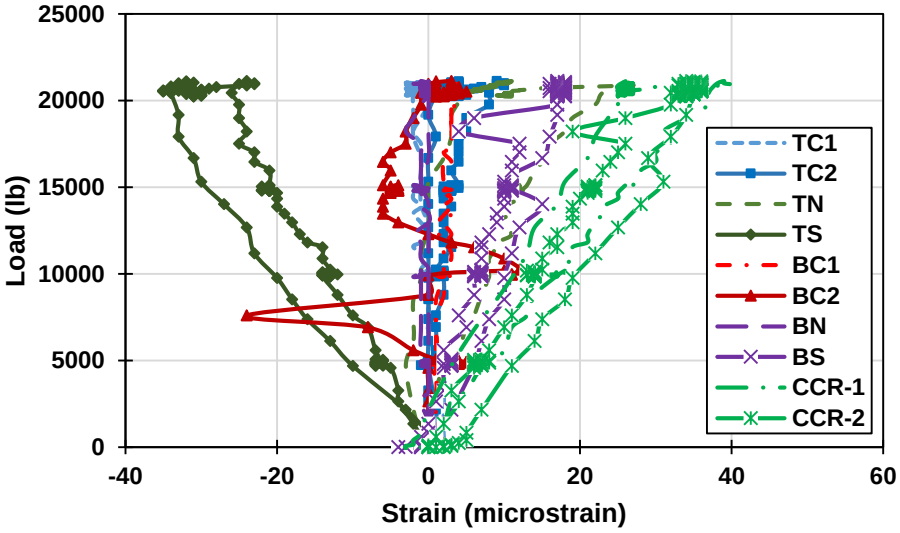

(a)

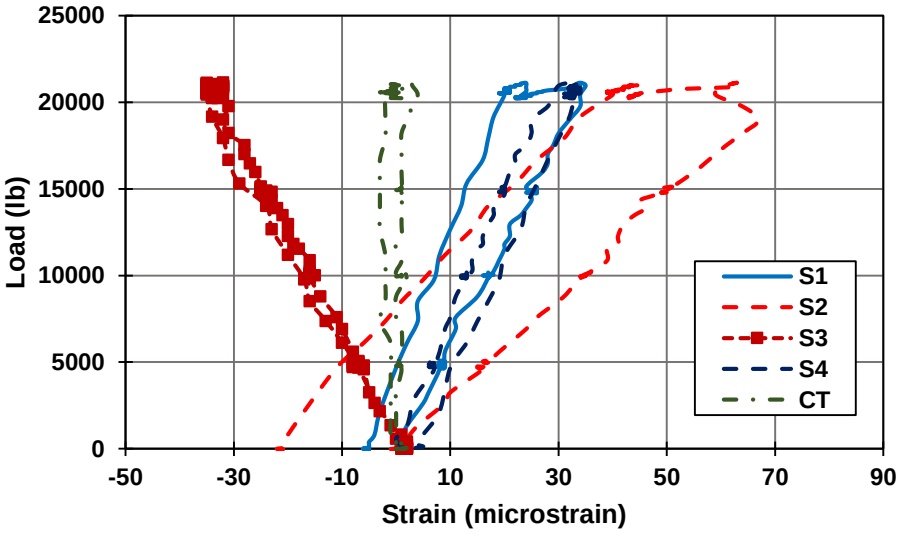

(b)

Figure 17. Load strains for (a) transverse rebar strains in top and bottom rebars and (b) surface strains at midspan for case 3

The strains recorded were in the transverse direction in the top and bottom reinforcing steel bars of the deck and are presented against loading recorded at the individual loading points. The strain recorded on all strain gauges were between positive and negative 40 microstrain. The strain distribution, however, provides insight into the unique behavior that the joint is performing under high shear force-induced loading.

The transverse strain at the center of the joint in the top reinforcing steel bar, i.e., TC1, was 10 microstrain for 21 kips loading, and, in the bottom reinforcing steel bar, i.e., BC1, it was 3 microstrain. The strain in the top reinforcing steel bar at the same cross section at the interface of the joint and the unrestrained beam, i.e., TN, was 27 microstrain, and, in the bottom reinforcing steel bar, i.e., BN for the unrestrained beam, it was negative 2 microstrain. The negative microstrain indicates compressive force. The strains at the interface of the joint and the unrestrained beam on top of the reinforcing steel bar, i.e., TS, showed a value of negative 27 microstrain, and the bottom strain gauge, i.e., BS, showed 17 microstrain.

These strain values highlight three unique stress distributions within the joint. On the interface between the UHPC joint and the restrained beam, the distribution is purely flexural with tensile stresses at the top and compressive stresses at the bottom. At the interface of the UHPC joint and the unrestrained beam, the direction of stresses is reversed with tensile stresses at the bottom and compressive stresses at the top. The stresses within the joint at the center are purely tensile on top and bottom, with stresses at the top reinforcing steel bar being three times more than that at the bottom reinforcing steel bar. This unique distribution can be attributed to the unique shape of the joint, as the ends of the joints are triangular sections pressing against two smaller triangles on the deck. This information provides more detailed insight into the behavior of the joint and can be helpful in determining any associated problems in the future.

The transverse strains recorded in the deck were also plotted (Figure 18).

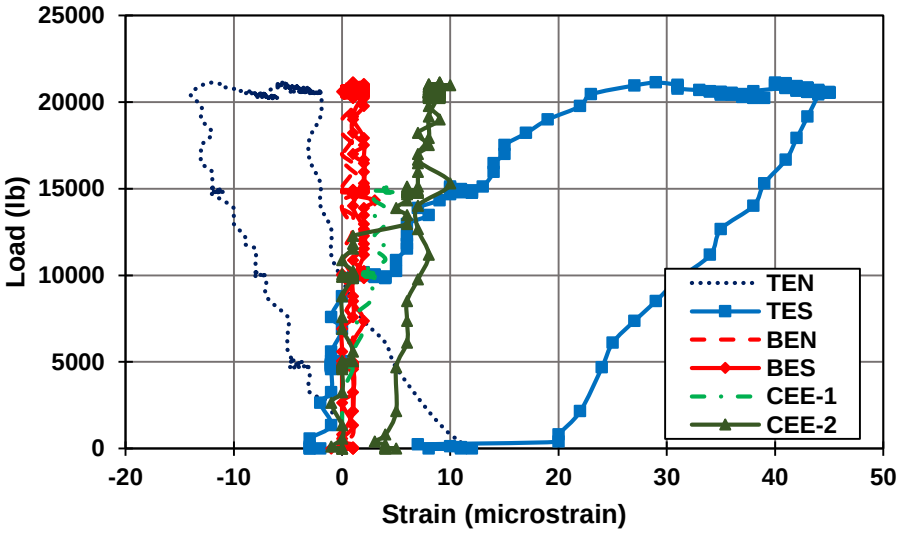

(a)

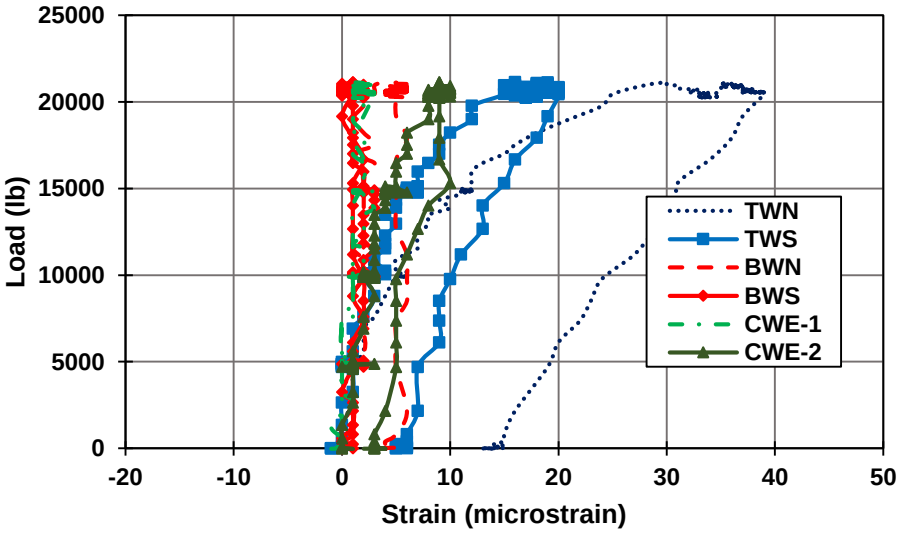

(b)

Figure 18. Transverse rebar strains at (a) east quarter span and (b) west quarter span for case 3

The strain in the top reinforcing steel bar, i.e., CCR-1 at the restrained beam, showed a strain of 39 microstrain and that on the unrestrained beam showed 34 microstrain at the loading value of 21 kips. The high value in the unrestrained deck compared to the strains in the joint was motivation to limit the investigation in this case to service limit only. Preliminary observations indicated that greater loading would result in cracking in the deck rather than in the joint.

The transverse strains on the top deck surface were also recorded (Figure 18(b)). The strain gauge on the restricted beam 1 was tensile while that on the unrestrained beam 2 was

compressive. The strain on both decks, i.e., S1 and S4, at the middle of the two beam decks were in tension and resulted in nearly the same strain. The strain on top of the joint was minimal, i.e., only 10 microstrain. This highlights the fact that the strain in the joint will be much less than the strain in the rest of the deck in all three cases. This could be attributed to the superior strength of the UHPC and the unique design of the joint, which resulted in twice as much steel as in the rest of the deck.

The strain in the quarter span followed the same trend as that at midspan (Figure 18). The TEN strain gauge showed unexpected results, as the results from the TWN, TWS, and TES gauges in the corresponding locations showed tensile strain, which is the expected result. The strains further showed that the entire joint was under shear loading along the entire span, as the strains in the top and bottom reinforcing steel bars in the joint were in tension.

3.4. Case 4. Testing of T-Beams for Individual Capacity

After testing the structure under service loading for joint capacity and structural integrity, the two T-beams were separated by cutting through the center of the specimen, creating two identical T-beam specimens. These two individual beams were tested by loading all four points at the same time on each individual beam. The loading from the four actuators was transferred to an I-beam placed under the actuators, and, then, a 10 × 10 in., 1.5 in.-thick steel plate transferred the load to the longitudinal centerline of the beam. This ensured the transfer of loading from the two actuators as one point load at the center of the beam. This loading arrangement helped in loading the beam symmetrically in the transverse direction.

Beams 1 and 2 both showed a smooth linear loading curve (Figure 19).

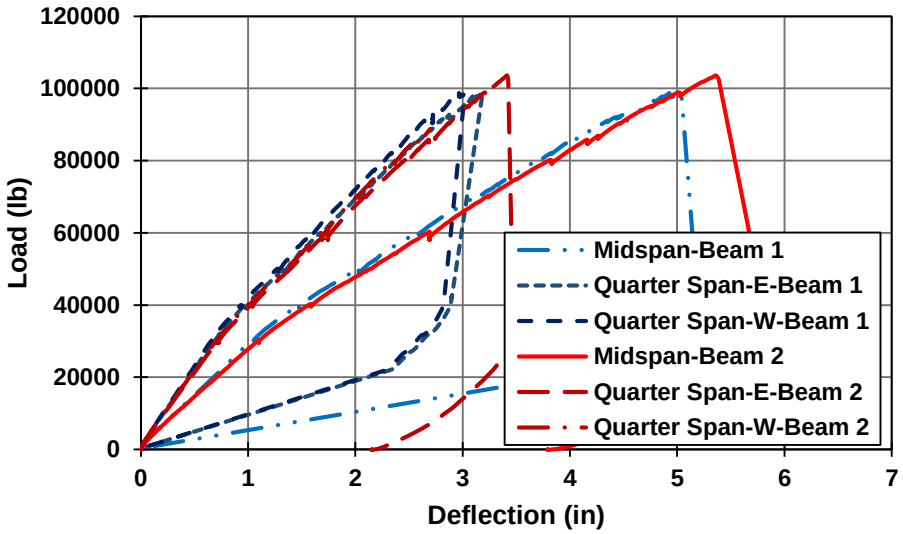

Figure 19. Load deflection comparison at ultimate stage

The load deflection curve at the individual loading point and the deflection at the bottom surface of the beam showed that the load deflection was linear up until 25 kips, after which the load deflection curve showed a change in the slope but stayed linear until the ultimate load. The ultimate load was the load at which the concrete under the loading point crushed. This load exceeded 100 kips in both beams. The unloading curve showed a sudden drop in the load at failure and then a residual deflection of 2.4 in. and 3.8 in. for beam 1 and beam 2, respectively.

The load deflection curves for the quarter span in both beams followed nearly identical paths. The change of slope occurred at about 25 kips in the quarter span load deflection curves as well, and then showed a linear response with a decreased slope until failure. The unloading curves followed smooth unloading paths with a residual quarter span deflection of 1.3 and 2.2 in. at the end of unloading. The two beams behaved in a nearly similar way as expected with only 3% variation in ultimate capacity. The load was plotted against compressive strain on top of the deck in beam 2 as shown in Figure 20.

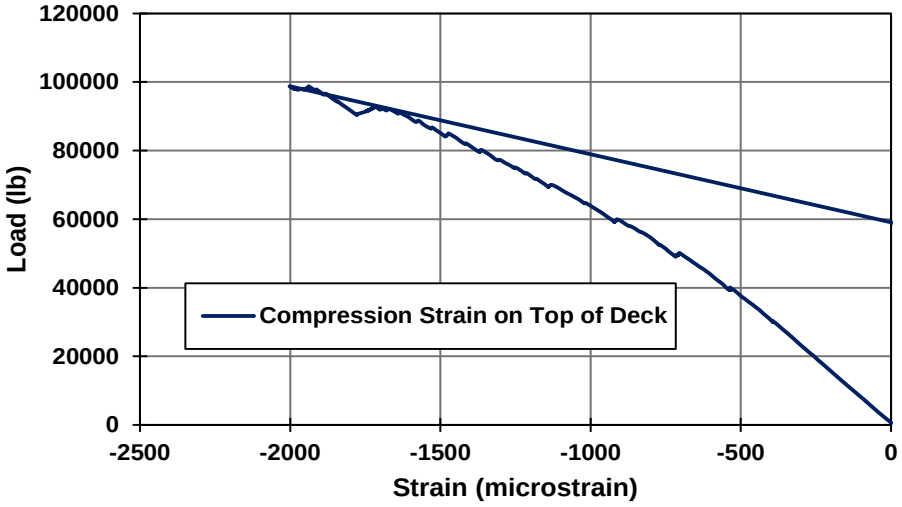

Figure 20. Load vs. compression strain at top deck for beam 1

The shear strains in the beams were monitored at a distance close to each support. Three BDI gauges were installed in the vertical, diagonal, and horizontal directions, as represented by VE, DE, and HE. The values were recorded only up to 40 kips loading. At 40 kips, a crack passed through the west horizontal BDI gauge, and, beyond that point, the recorded strain values would not have been accurate; thus, all BDI gauges were detached. The resulting strain values are presented in Figure 21. The E represents the east end BDI gauges, and W represents the west end BDI gauges.

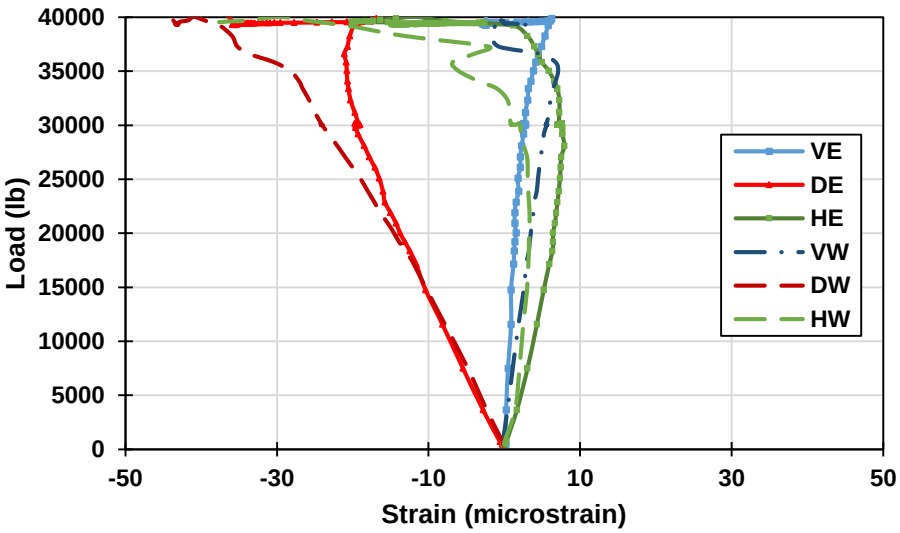

Figure 21. Shear strain at supports on the side of beam 1

The vertical and horizontal strains were tensile while the diagonal strain was compressive until 30 kips, after which all strains started to vary unexpectedly, which indicates cracks passing through these BDI gauge locations.

The cracking in both beams are shown and color coded in Figure 22.

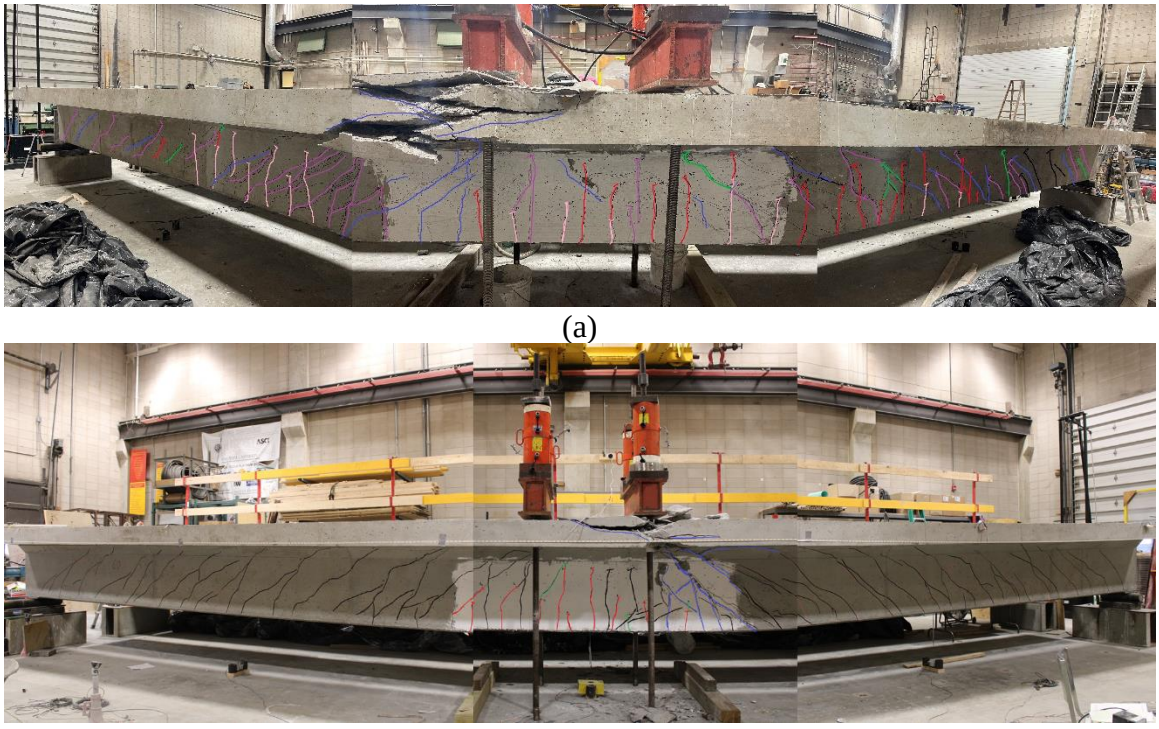

(a)

(b)

Figure 22. Crack maps for (a) beam 1 and (b) beam 2 at ultimate stage

The cracking in both beams started as flexural cracks. In beam 1, the first cracking was observed at a loading value of 20 kips, shown with pink lines in the figure. The cracks were observed between the loading points, as well as outside the two loading points.

On further loading, the existing cracks extended toward the top, and some new cracks developed/became apparent. These cracks are marked at 30 kips loading with red lines. Most of these cracks were flexural, but shear cracks started to appear as well.

The beams were further loaded to 40 kips and the cracks were marked with green lines. As shown, the existing cracks extended, and a couple of shear cracks appeared.

On further loading up to 50 kips, shear cracks started appearing along the entire length of the beam with more flexural cracks appearing between the two loading points. The cracks at this loading level are marked as purple lines.

The cracks at 60 kips loading are represented with black lines, and the blue lines represent the cracking marked at ultimate loading after the failure. The failure path shows that the deck failed in compression under the loading point, and the failure path extended down to the beam.

In beam 2, the first cracking, as shown with red lines, was observed at 30 kips loading. This was seen in the load deflection curve, as well, given the load deflection curve slope changes after 30 kips. Four flexural cracks occurred between the loading points, and three shear cracks emerged from the bottom of the beam right next to the loading point. Three of these cracks were on the west side of the beam, where the roller support was located, and one was on the east side, where a pin support was located.

On further loading, the existing cracks widened and extended further. The cracks marked with green lines were at 40 kips loading. The already existing cracks widened, and a few new cracks also emerged.

Upon further loading, shear cracks started to appear along the entire length of the beam. The black lines show the cracking at 60 kips loading. The excessive shear cracks made it difficult to mark cracks at loads greater than 60 kips.

All cracks kept widening until failure. The crushing path and cracking at the end of loading is shown in blue in the figure. The failure occurred by compression of the concrete under the loading point. The failure path extended down to the beam similar to what was observed in beam 1.

4. NUMERICAL INVESTIGATIONS

To further understand the effects of material of choice and detailing on the behavior of the joint, the researchers created a set of FE models using the Abaqus software package. The models were validated utilizing the results from the experimental tests.

The concrete T-beams and UHPC joint were modeled using eight-node solid elements with an enhanced hourglass control. The reinforcing steel bars were modeled as two-dimensional (2D) truss elements. The contacts between the UHPC joint and the concrete decks were tie constraints. This type of constraint does not allow any relative movement between the two surfaces in contact. The model geometry was the exact representation of the specimen built in the laboratory. The loading points were replicated using steel plates that were 30.48 cm × 30.48 cm (12 in. × 12 in.) to avoid stress concentration at the loading points. The model is shown in Figure 23.

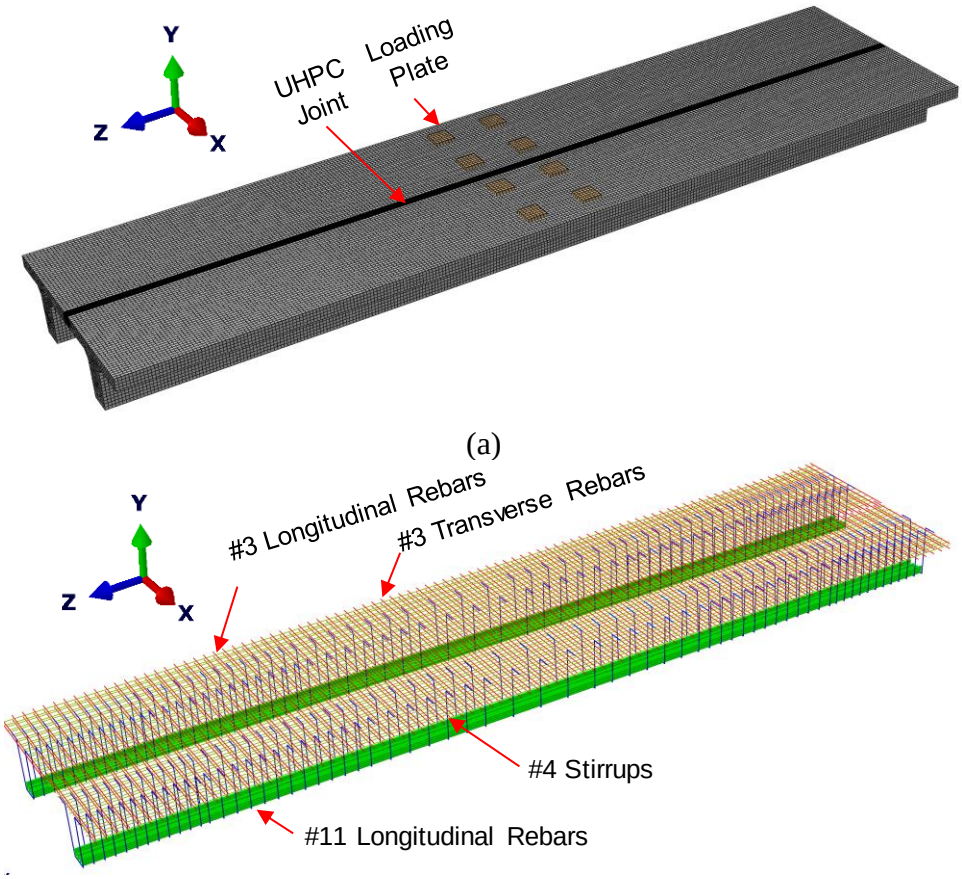

Figure 23. FE model for (a) structure and (b) rebar cage

The concrete and UHPC were modeled using concrete damaged plasticity. The steel reinforcing steel bars were modeled accounting for the plastic behavior of the reinforcing steel bars as reported by Abed et al. (2020).

4.1. Validation

The experimental data were utilized to validate the FE models created for the experimental setup. The models showed close comparison to the recorded deflection values from the experiment, confirming an accurate replication of the actual tested specimen. The comparison of results for case 1 is shown in Figure 24.

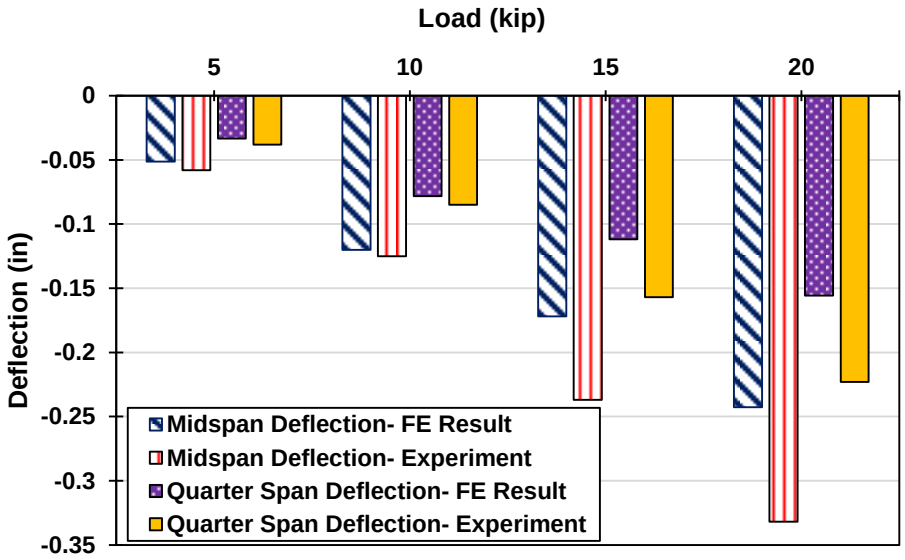

Figure 24. Comparison of FE and experimental results for case 1

The figure shows that the deflection values recorded were within 3–27% for the midspan deflections. The FE simulations were used to explore two main parameters: the behavior of the joint under the service limit load of an actual HL-93 truck placed on one beam to maximize shear strain and the behavior of the individual beams under an actual HL-93 truck.

4.2. Behavior of Joint under HL-93 Truck Loading

To explore the joint behavior, the HL-93 truck was placed on only one beam to see the joint behavior under maximum shear stress. Two cases were investigated for this purpose: both beams' vertical movement left unrestrained, i.e., the simulation named unrestrained beam (UB), and one beam's vertical movement restrained, i.e., the results named restrained beam (RB).

In these FE simulations, HL-93 is a full truck with 14 ft spacing between the front, mid, and rear wheels, length-wise. Each set of wheels was spaced at 6 ft apart transversely. The full truck was placed to create the maximum moment under HL-93 truck loading. The center wheel was placed at midspan and the front and rear wheel at 14 ft distance from the midspan. The resulting behavior is compared in Figure 25.

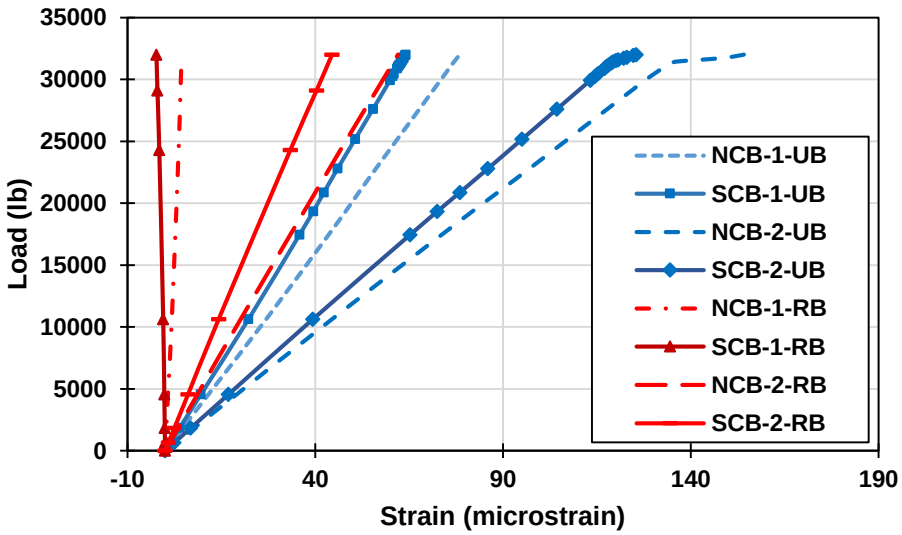

Figure 25. Bottom rebar strain comparison for unrestrained beam (UB) and restrained beam (RB)

In the figure, UB refers to beam with case where both beams are free to deflect, and RB refers to the case where beam 1 is restricted from vertical movement. The loading truck was placed only on beam 2. The strains in the north beam are numbered 1 and in the south beam number 2. NCB-1 and SCB-1 are in beam 1 and NCB-2 and SCB-2 are in beam 2. All of the strain labels are the same as the strain gauges in Chapter 2.

As the figure shows, the strains recorded for the UB case were greater than the strains for the RB case, as expected. Furthermore, the strains in beam 2 were always greater than the strains in beam 1, as the truck load was placed on beam 2.

The results for transverse reinforcing steel bar strains in the joint at the midspan cross section are presented in Figure 26.

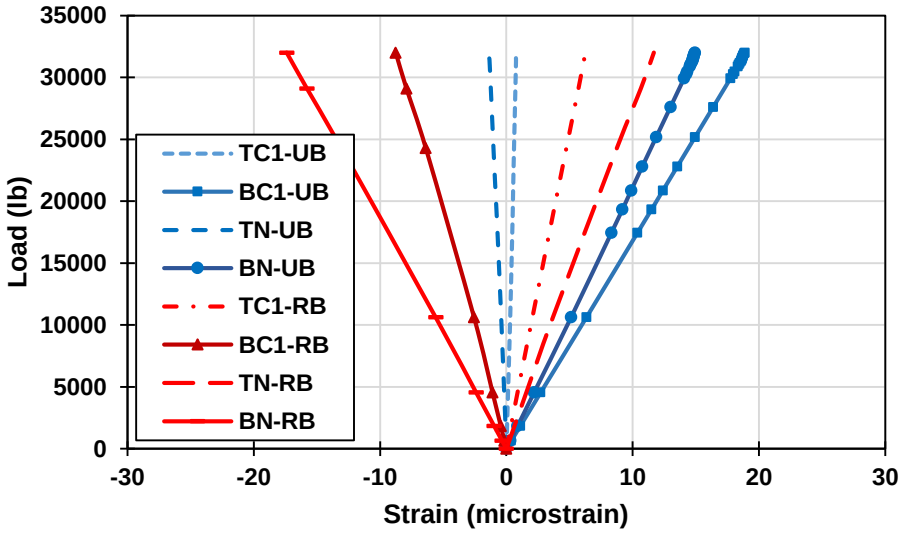

(a)

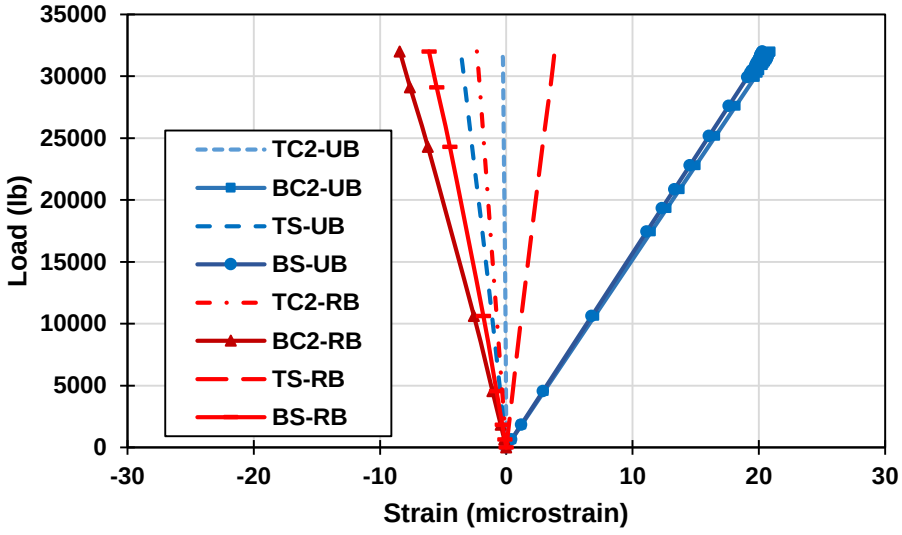

(a)

Figure 26. Rebar strains at the midspan cross section of the beams

Figure 26(a) presents the strains recorded in beam 1 in the UB and RB case. Figure 26(b) presents the strains in beam 2. In the UB condition, the strains in the center of the joint, TC1 and BC1 were tensile, with the bottom reinforcing steel bar tensile strain greater than that of the top reinforcing steel bar, showing an axial pull with varying magnitude on the top and bottom reinforcing steel bars. In the RB case, the strains recorded in TC1 was tensile, while that in BC1 was compressive, showing a pure flexural behavior at the center. This observation shows that, in a realistic situation (i.e., UB), the joint at center will be under axial loading.

The strains at the interface of the joint have the top reinforcing steel bars in compression while the bottom reinforcing steel bars are in tension for beam 1 in both the UB and RB condition. The compressive strains in the top reinforcing steel bars are greater for the RB condition, and tensile

strains in the bottom condition are less. This could be explained by the fact that, in the RB condition, beam 1's vertical movement is restricted; thus, the top reinforcing steel bars undergo a greater compression strain.

The transverse reinforcing steel bar strain results for beam 1 were complemented by the transverse reinforcing steel bar strain for beam 2 at the same cross section. The strains at the center of the joint, TC2 and BC2, for the UB condition resulted in similar strains as those for beam 1. The magnitudes were a little higher, i.e., the magnitude for TC1 was 19 microstrain and that for TC2 was 21 microstrain.

The strains for the interface of the joint and the beam, TS and BS, for the UB condition followed the same pattern as that for beam 1, with the top reinforcing steel bars in compression and the bottom ones in tension.

The strains at center for the RB condition had interesting behavior with TC2 and BC2 both recording compressive strains and the top reinforcing steel bars showing lower strain values than the bottom reinforcing steel bars while the top reinforcing steel bars for beam 1 were in tension. TS and BS followed the same pattern as that for beam 1 with TS in tension and BS in compression, with slightly lower magnitude than what was recorded for beam 1 in the RB case. These strain values suggest that the joint, while creating a continuous system, keeps its own unique rigid behavior and acts as a pivot around which both beams rotate. This results in pure axial strains at the center of the joint and flexural behavior at the interface between the UHPC joint and the concrete deck.

The strain recorded in the top reinforcing steel bars at the center of both concrete decks further provides insight into the strain distribution in the deck. It can be seen that, under service limit loading, the greatest strains occur in the deck rather than the joint (Figure 27).

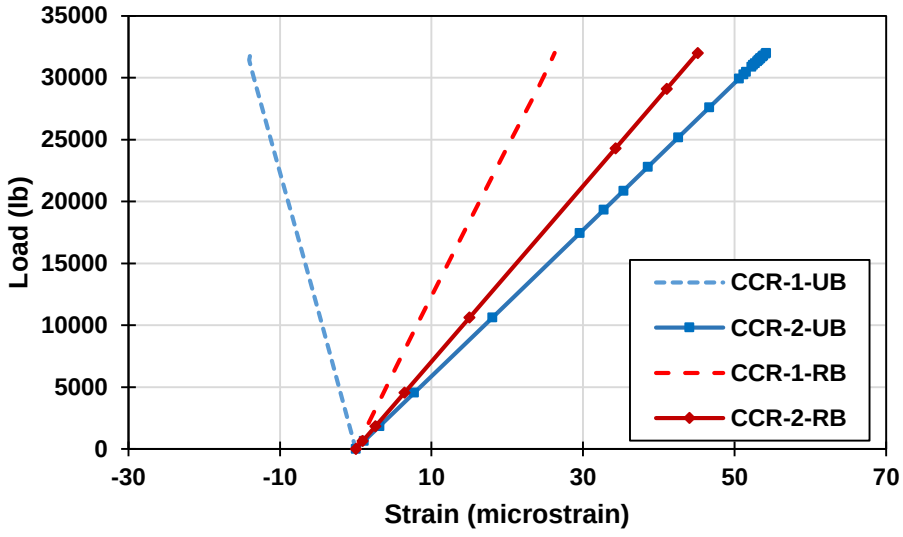

Figure 27. Top rebar strains in the middle of the deck for the UB and RB cases

The strains recorded in the deck in the unloaded beam were about three times of that recorded in the joint, i.e., the strains recorded in the joint were 19 microstrain and that on the deck were 55 microstrain. This is for both the UB and RB case, with the UB case resulting in more strain than the RB case. Another important observation was that the strains in the UB case were greater than in the RB case, i.e., for CCR-2, the strain in the UB case was 55 microstrain, while that in the RB case was 45 microstrain. This could be explained by the fact that the deflections of the UB setup was greater than the deflection experienced by the RB setup.

4.3. Behavior of Individual T-Beams under HL-93 Loading

The behavior of the individual T-beams was investigated with the HL-93 truck middle wheel placed at midspan and the front and rear wheels at 14 ft from the midspan. The truck loading results are presented in Figure 28.

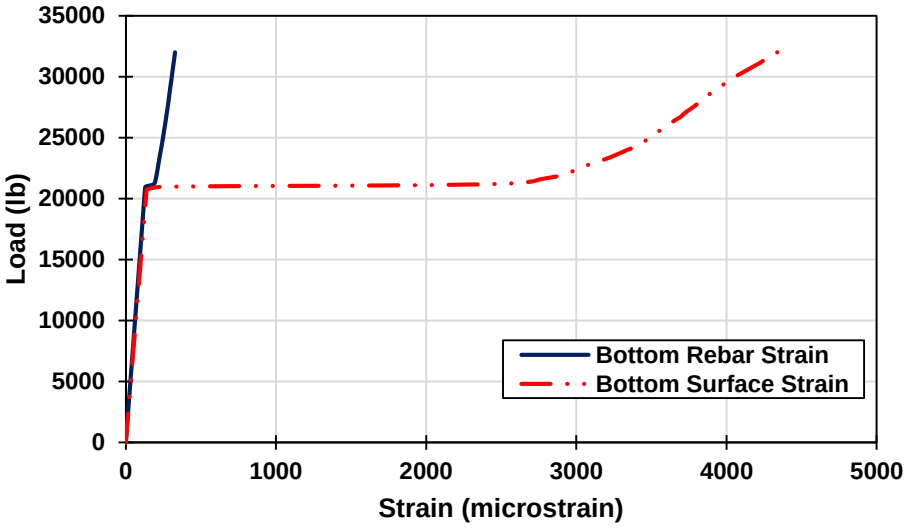

Figure 28. Load strain for bottom rebar at midspan

The strain recorded at the bottom reinforcing steel bars and the bottom surface of the beam at midspan were plotted against the wheel load at midspan. The results showed that the initial cracking started at a 21 kips wheel load. Upon further loading, more cracks appeared. As Figure 29 shows, the number of cracks was larger on the side with the 16 kips loading (i.e., total 32-kip loading divided between two locations).

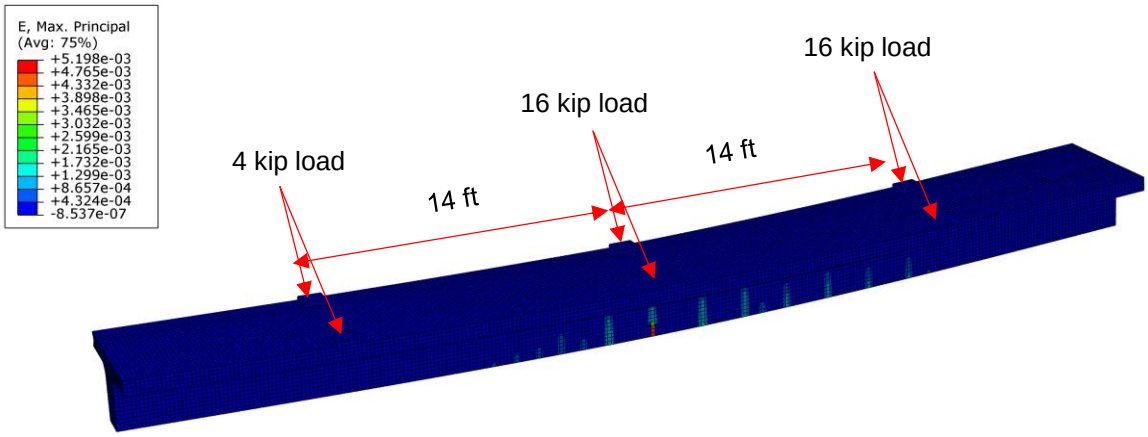

Figure 29. Effect of HL-93 loading on single T-beam bridge

The results showed that the beams exhibit some cracking under the HL-93 truck loading when they are individually loaded. This was observed in the experiment as well when the beams showed initial cracking at 20 kips of loading. However, it is essential to keep in mind that, as a system, the entire bridge did not show any cracking under the maximum load required to generate the maximum moment with 32 kips loading. As a full T-beam system bridge, the moments will be distributed among the two T-beams, thus resulting in double the capacity of a single tested T-beam.

5. CONCLUSIONS

A full-scale experiment and a set of FE simulations were carried out to investigate the behavior of an innovative T-beam bridge design with a unique longitudinal UHPC joint. The two T-beams were reinforced with high-strength, corrosion-resistant reinforcing steel bars. The joint detailing was unique as the joint had no longitudinal reinforcing steel bars and the reinforcement in the joint was extended from the deck into the joint.

The full-scale test setup was 46 ft long and 24 ft wide. The joint was tested under static flexural and shear stress under service limit loading. The T-beams were then separately tested to investigate their individual capacity and behavior. The experimental test results were complemented by a set of FE simulations that were used to investigate the behavior of full system and individual T-beams under HL-93 truck loading.

5.1. Conclusions from the Experimental Work

The following conclusions can be drawn from the experimental tests in the laboratory:

- The UHPC longitudinal joint was tested under flexure to have tensile stress on top and compressive stress at the bottom face of the joint. This was achieved by loading the two beams at 18 in. from the outer edges. This case was named case 1. The load deflection curves and the load strain curves for deflections at the bottom of the beams at midspan and the strains at the bottom reinforcing steel bars of the beams showed that, within the service limit, the beams were in linear elastic range with a small change in slope at 10 kips. No visible cracks were observed within the service limit under the loading condition of case 1.

- The transverse strains in the reinforcing steel bars in the UHPC joint were recorded to evaluate the performance of the joint. The resulting strains recorded in the top and bottom reinforcing steel bars of the joint showed that the strains in the joint were tensile on both the top and bottom reinforcing steel bars. This highlights the fact that the beam centerline acts as pivot for the load, and the inner flanges of the beams pull axially on the joint in tension. These results were further proved by the strains observed on the surface of the concrete decks. All of the strains in the joint and on the top surface of the deck were also tensile. The DCDTs mounted on the top and bottom surfaces of the joint did not record a crack, and no visible cracks were seen at the end of loading for case 1.

- The transverse strains were recorded at cross section quarter spans on both sides of midspan. The strains in the joint showed that the strains in the corresponding locations in the joint and the deck followed the same trend as the strains at midspan. The tensile strains in the top reinforcing steel bars were about a third of the strains in the top reinforcing steel bars at midspan. This highlights the fact that, when moving away from the loading points, the strains in the joint in the transverse direction decrease, but the general behavior of the longituddinal joint throughtout the length remains the same.

- The bridge system was tested to have tensile stresses at the bottom surface of the UHPC joint and compressice stresses at the top surfaces of the joint. The loads were applied 18 in. from the centerline of the joint. The loading in this case was flexural. The load deflection and load strains curves for deflection at midspan and quarter span and strains at the bottom reinforcing steel bars at midspan showed a linear elastic behavior. The unloading curve showed smooth unloading with negligible residual deflection. This indicated that, within service limit loading, the system behaved as linear elastic with no visible cracking anywhere on the beams.

- The transverse strains in the top and bottom reinforcing steel bars of the UHPC joint were recorded at midspan to investigate the behavior of the joint. The strains recorded in the top reinforcing steel bars were compressive and they were tensile in the bottom reinforcing steel bars. The compressive strains at the center of the joint were less than half of those at the interface of the joint and the concrete beam. The tensile strains at the center of the bottom reinforcing steel bars were only 10% lower than those at the interface of the UHPC joint and the concrete beams. The lower strain at the center under flexure in case 1 and case 2 can be explained by their associated development lengths. The shorter development length may result in less strain, but no signs of slips or separation of joints were observed in either case 1 or case 2 under flexural loading.

- The transverse strains were recorded at the quarter span for case 2 as well. The resulting strains at corresponding locations followed the same trend as the strains recorded at midspan. Both compressive and tensile strains at the top and bottom reinforcing steel bars, respectively, were about half of the strains at midspan. The strains trend did not change either. The DCDTs mounted at midspan and quarter span did not record any cracks, and no cracks were seen with visual inspection during or after the loading.

- The bridge system was tested to exert maximum shear stress in the UHPC joint. This was achieved by restricting the vertical movement of one of the beams and loading all of the loading points on the other beam. This loading arrangement was named case 3. The load deflection and load strain curves showed that the unrestrained beam behaved linear elastically until 15 kips and showed a small change in slope after that, but stayed linear with reduced slope until the service limit loading of 21 kips. The deflection and strain for the movement-restricted beams were negligible, indicating that the supports restricting the movement were performing as intended.

- The transverse strains in the joint were recorded for case 3. The strains at the center of the joint were tensile in both the top and bottom reinforcing steel bars. The strains at the interface of the UHPC joint and the restrained beam were tensile and those in the bottom reinforcing steel bars at the same section were compressive. The strains at the interface of the joint and the unrestrained beam at the top reinforcing steel bar was in compression and bottom reinforcing steel bar in tension. This highlights a unique distribution of strain in the joint, which can be explained by the shape of the joint. Under shear force, the triangural shape of the joint is pushing downward on the bottom triangle of the restrained beam. In the unrestrained beam, the traingular part of the joint is pushing upwards on the top triangle of

the T-beam. Thus, careful consideration must be given during detailing of the joint, although the current detailing showed no damage to the joint for service limit loading.

- The strains recorded at quarter span also followed the same trends as those for midspan for case 3. The strains at quarter span were, however, almost the same as those for midspan, unlike case 1 and 2, where the strains were almost half of the strains at midspan. This suggested that the entire section was under similar shear stress in the joint. The DCDTs on the top and bottom of the joints showed no cracks, and no cracks were seen during or after loading. The joint and entire system kept its integrity under flexural and shear loading.

- The two T-beams were separated by cutting through the joint and tested under flexural loading until failure. The load deflection curves for beam 1 and beam 2 followed the same path, varying only 3% at ultimate capacity. Beam 1 showed ultimate capacity at 400 kips (i.e., 100 kips at each loading point), and beam 2 showed ultimate capacity at 412 kips (i.e., 103 kips at each loading point). The beams showed a similar load deflection response for deflections at midspan as well as quarter span.

- Cracking in the individual beams started appearing as the applied load increased. The intial cracks were flexural cracks but, upon further loading, shear cracks started to appear. At 50 kips loading for beam 1 and 60 kips for beam 2, shear cracks formed along the entire length of the beam. The beams failed by compression failure of the concrete under the loading points in both beams. The strain at the top surface of beam 1 at failure was 2,000 microstrain. The cracking at 20 kips loading in the individual beams suggested that the individual beams may observe some cracking under the HL-93 truck maximum loading configuration.

5.2. Conclusions from the Numerical Investigation

The experimental data were utilized to validate the FE models created using the Abaqus software package. The FE models were further explored by placing a full HL-93 truck on the full-scale tested specimen with the UHPC joint and on each of the individual beams. The simulations on the full-scale specimen included two further cases: in the first case, both beams were unrestrained, and, in second case, one of the beam's vertical movement was restrained similar to case 3. The T-beams were individually explored for their behavior under the loading of a full HL-93 truck on the beam. The following conclusions can be drawn from the numerical simulations:

- The unrestrained and restrained beam cases were compared. The comparison of load deflection curves for deflection at midspan and load strain curves for strains at the bottom reinforcing steel bars of the midspan showed that the strains for the unrestrained case were greater than that for the restrained case. This could be explained by the fact that the entire system deflected more when unrestrained, thus resulting in lower strains at the bottom reinforcing steel bars.

- In the unrestrained beam case, the transerve strains at the center of the joint at midspan were tensile in both the top and bottom reinforcing steel bars, while, in the restrained beam case, the top reinforcing steel bars are in tension with the bottom reinforcing steel bars in compression. This highlights the fact that, in a realistic situtation, there will be a sideways pull on the joint rather than a bending in the joint in transverse direction. The strains in the interface of the UHPC joint and unloaded beam has top reinforcing steel bars in comrpession and bottom reinforcing steel bars in tension, suggesting that the joint is bending along the interface of the unloaded beam and the UHPC joint. The strain observed at the interface of the UHPC joint and the loaded beam showed that the top reinforcing steel bars are in compression in the unrestrained beam case and in tension in the restrained beam case. The bottom reinforcing steel bars are in tension in the unrestrained beam case and in comrpession in the restrained beam case. In both cases, the joint behaved as a separate rigid entity around which the two T-beams were bending; however, the unrestrained beam case presents a more realistic situation. The strains at the center of the joint in the unrestrained beam case were a fifth of the tensile strains of the restrained beam case.

- The comparison of strains in the deck and the joint revealed that, in both the unrestrained beam and restrained beam cases, the strains in the joint were much less than the strains observed in the deck. The tensile strains in the top reinforcing steel bars of the deck were twice that of strains in the joint. The strains in the restrained beam case were 18% lower than those for the unrestrained beam case in deck 2. This could be associated to the fact that, in the UB case, the loaded beam deflected more than in the restrained beam case, resulting in greater strains in the deck.

- The individual T-beams were also studied by placing the HL-93 truck to generate maximum moment. The first cracking started to happen at 21 kips wheel loading, and the reinforcing steel bar strain showed yielding as well. This showed that the individual T-beams experience some cracking under an HL-93 truck load when placed to generate the maximum positive moment in the beam. However, it should be kept in mind that, when they are part of a full system, there are no cracks, as observed in both the experiment and in the simulations performed for the unrestrained beam and restrained beam cases.

REFERENCES

Abed, F., A. Abdul-Latif, and G. Z. Voyiadjis. 2020. Performance of MMFX Steel Rebar at Elevated Temperatures. *Journal of Engineering Mechanics*, Vol. 146, No. 11.

Baer, C. 2013. *Investigation of Longitudinal Joints between Precast Prestressed Deck Bulb Tee Girders Using Latex Modified Concrete*. University of South Carolina, Columbia, SC.

Bohn, L. M. 2017. Rehabilitation of Longitudinal Joints in Double-Tee Girder Bridges. MS thesis. South Dakota State University. Brookings, SD.

DeJong, A., W. Shi, B. Shafei, and T. Hosteng, T. (2021) Integral Abutment Connections with Grouted Reinforcing Bar Couplers and Ultra-High Performance Concrete. *Journal of Bridge Engineering*, Vol. 26, No. 8, pp. 1–15.

Dopko, M., M. Najimi, B. Shafei, X. Wang, X., P. Taylor, and B. Phares. 2018. Flexural Performance Evaluation of Fiber Reinforced Concrete Incorporating Multiple Macro-Synthetic Fibers. *Transportation Research Record: Journal of the Transportation Research Board*, Vol. 2672, No. 27, pp. 1–12.

———. 2020. Strength and Crack Resistance of Carbon Microfiber Reinforced Concrete. *ACI Materials Journal*, Vol. 117, No. 2, pp. 11–23.

Dougherty, L. M., E. K. Cerreta, G. T. Gray, III, C. P. Trujillo, M. F. Lopez, K. S. Vecchio, and G. J. Kusinsk. 2009. Mechanical Behavior and Microstructural Development of Low-Carbon Steel and Microcomposite Steel Reinforcement Bars Deformed under Quasi-Static and Dynamic Shear Loading. *Metallurgical and Materials Transactions A*. Vol. 40A, pp. 1835–1850.

El Shahawy, M. 1990. Feasibility Study of Transversely Prestressed Double Tee Bridges. *Precast/Prestressed Concrete Institute (PCI) Journal*, Vol. 35, No. 5, pp. 56–96.

Frosch, R. J., S. Labi, and C. Sim. 2014. *Increasing Bridge Deck Service Life: Volume I—Technical Evaluation.* Joint Transportation Research Program, Purdue University, West Lafayette, IN.

Gong, L., D. Darwin, J. Browning, and C. E. Locke, Jr. 2002. *Evaluation of Mechanical and Corrosion Properties of MMFX Reinforcing Steel for Concrete*. University of Kansas Center for Research, Inc., Lawrence, KS.

Graybeal, B. A. 2010. *Behavior of Field-Cast Ultra-High Performance Concrete Bridges Deck Connections under Cyclic and Static Loading*. FHWA-HRT-11-023. Federal Highway Administration, Office of Infrastructure Research and Development, McLean, VA.

———. 2014. *Design and Construction of Field-Cast UHPC Connections*. Tech Note. FHWA-HRT-14-084. Turner-Fairbank Highway Research Center, Federal Highway Administration, McLean, VA.

Gulyas, R. J., G. J. Wirthlin, and J. T. Champa. 1995. Evaluation of Keyway Grout Test Methods for Precast Concrete Bridges. *Precast/Prestressed Concrete Institute (PCI) Journal*, Vol. 40, No. 1, pp. 44–57.

Jones, H. L. 2001. *Lateral Connections for Double Tee Bridges*. Texas Transportation Institute, Texas A&M University, College Station, TX.

Jones, J., K. Ryan, and M. "S." Saidi. 2015. *Toward Successful Implementation of Prefabricated Deck Panels to Accelerated Bridge Construction Process*. Center for Civil Engineering Earthquake Research, University of Nevada, Reno, NV.

Karim, R. and B. Shafei. 2021a. Performance of Fiber-Reinforced Concrete Link Slabs with Embedded Steel and GFRP Rebars. *Journal of Engineering Structures*, Vol. 229, pp. 1–12.

———. 2021b. Flexural Response Characteristics of Ultra-High Performance Concrete Made with Steel Microfibers and Macrofibers, *Journal of Structural Concrete* [In Press].

Karim, R., M. Najimi, and B. Shafei. 2019. Assessment of Transport Properties, Volume Stability, And Frost Resistance of Non-Proprietary Ultra-High Performance Concrete. *Journal of Construction and Building Materials*, Vol. 227, pp. 1–10.

Khatami, D. and B. Shafei. 2021. Impact of Climate Conditions on Deteriorating Reinforced Concrete Bridges in the U.S. Midwest Region. *Journal of Performance of Constructed Facilities*, Vol. 35, No. 1, pp. 1–11.

Khatami, D., S. Hajilar, and B. Shafei. 2021. Investigation of Oxygen Diffusion and Corrosion Potential through a Cellular Automaton Framework. *Journal of Corrosion Science*, Vol. 187, 109496, pp. 1–10.

Liu, Z., B. M. Phares, W. Shi, and B. Shafei. 2020. Full-Scale Evaluation of an Innovative Joint Design between Adjacent Box Beams. *Transportation Research Record: Journal of the Transportation Research Board*, Vol. 2674, No. 2, pp. 33–44.

Martin, L. D. and A. E. N. Osborn. 1983. *Connections for Modular Precast Concrete Bridge Decks*. Federal Highway Administration, Engineering Research and Development Bureau, Washington, DC.

Oppong, K., D. Saini, and B. Shafei. 2021. Ultra-High Performance Concrete for Improving Impact Resistance of Bridge Superstructures Prone to Over-Height Vehicle Collision. *Journal of Bridge Engineering*, Vol. 26, No. 9, pp. 1–8.

Peruchini, T. J., J. Stanton, and P. Calvi. 2017. *Investigation of Ultra-High Performance Concrete for Longitudinal Joints in Deck Bulb Tee Bridge Girders*. Washington State Transportation Center (TRAC), University of Washington, Seattle, WA.

Phares, B. M., L. Greiman, and Z. Liu. 2015. *Evaluation of the Need for Longitudinal Median Joints in Bridge Decks on Dual Structures*. Bridge Engineering Center, Iowa State University, Ames, IA. https://intrans.iastate.edu/app/uploads/2018/03/longitudinal_deck_investigation_w_cvr.pdf.

Shafei, B., M. Kazemian, M. Dopko, and M. Najimi. 2021. State-of-the-Art Review of Capabilities and Limitations of Polymer and Glass Fibers used in Fiber-Reinforced Concrete. *Journal of Materials*, Vol. 14(2), No. 409, pp. 1–44.

Sharp, S. R. and A. K. Moruza. 2009. *Field Comparison of the Installation and Cost of Placement of Epoxy-Coated and MMFX 2 Steel Deck Reinforcement: Establishing a Baseline for Future Deck Monitoring*. Virginia Transportation Research Council, Charlottesville, VA.

Sharp, S. R., L. J. Lundy, H. Nair, C. D. Moen, J. B. Johnson, and B. E. Sarver. 2011. *Acceptance Procedures for New and Quality Control Procedures for Existing Types of Corrosion-Resistant Reinforcing Steel*. Virginia Center for Transportation Innovation and Research, Charlottesville, VA.

Shi, W., B. Shafei, Z. Liu, and B. M. Phares. 2019. Early Age Performance of Longitudinal Bridge Joints Made with Shrinkage Compensating Cement Concrete. *Engineering Structures*, Vol. 197. pp. 1–11.

Shi, W., B. Shafei, Z. Liu, and B. M. Phares. 2020a. Longitudinal Box-Beam Bridge Joints Under Monotonic and Cyclic Loads. *Engineering Structures*, Vol. 220, pp. 1–11.

Shi, W., M. Najimi, and B. Shafei. 2020b. Chloride Penetration in Shrinkage-Compensating Cement Concretes. *Journal of Cement and Concrete Composites*, Vol. 113, pp. 1–11.

———. 2020c. Reinforcement Corrosion and Transport of Water and Chloride Ions in Shrinkage-Compensating Cement Concretes. *Journal of Cement and Concrete Research*, Vol. 135, pp. 1–9.

Wehbe, N., M. Konrad, and A. Breyfogle. 2016. Joint Detailing between Double Tee Bridge Girders for Improved Serviceability and Strength. *Transportation Research Record: Journal of the Transportation Research Board*, No. 2592, pp.108–116.

Wenzlick, J. D. 2006. *Evaluation of Very High Strength Latex Modified Concrete Overlays*. Missouri Department of Transportation, Jefferson City, MO.

THE INSTITUTE FOR TRANSPORTATION IS THE FOCAL POINT FOR TRANSPORTATION AT IOWA STATE UNIVERSITY.

InTrans centers and programs perform transportation research and provide technology transfer services for government agencies and private companies;

InTrans contributes to Iowa State University and the College of Engineering's educational programs for transportation students and provides K–12 outreach; and

InTrans conducts local, regional, and national transportation services and continuing education programs.

IOWA STATE UNIVERSITY

Visit **InTrans.iastate.edu** for color pdfs of this and other research reports.